arXiv:1409.7920v2 [nucl-th] 10 Mar 2016

2π production in the Giessen coupled-channels model. *

V. Shklyar,† H. Lenske, and U. Mosel

Institut für Theoretische Physik, Universität Giessen, D-35392 Giessen, Germany

The coupled channels Lagrangian approach underlying the Giessen model (GiM) is extended to describe the $\pi N \to \pi N$, $2\pi N$ scattering in the resonance energy region. As a feasibility study we investigate single and double pion production up to the second resonance region. The $2\pi N$ production has been significantly improved by using the isobar approximation with σN and $\pi\Delta(1232)$ in the intermediate state. The three-body unitarity is maintained up to interference pattern between the isobar subchannels. The scattering amplitudes are obtained as a solution of the Bethe-Salpeter equation in the K matrix approximation. As a first application we perform a partial wave analysis of the $\pi N \to \pi N$, $\pi^0\pi^0 N$ reactions in the Roper resonance region. We obtain $R_{\sigma N}(1440) = 27^{+4}_{-9}\,\%$ and $R_{\pi\Delta}(1440) = 12^{+5}_{-3}\,\%$ for the σN and $\pi\Delta(1232)$ decay branching ratios of $N^*(1440)$ respectively. The extracted πN inelasticities and reaction amplitudes are consistent with the results from other groups.

PACS numbers: 11.80.-m,13.75.Gx,14.20.Gk,13.30.Gk

I. INTRODUCTION

The investigation of properties of nucleon resonances remains one of the primary goals of modern hadron physics. The main information about the hadron spectra comes from the analysis of scattering data. Coupled-channel approaches have proven to be an efficient tool to extract baryon properties from experiment. The Giessen coupled-channel model (GiM) [1–9] has been developed for a combined analysis of $(\pi/\gamma)N \to \pi N$, $2\pi N$, ηN, ωN $K\Lambda$, $K\Sigma$ reactions to extract properties of nucleon resonances from pion- and photon-induced reactions.

* Supported by Transregio SFB/TR16, project B.7

†Electronic address: shklyar@theo.physik.uni-giessen.de

Since the $\pi N \to 2\pi N$ reaction could account for up to 50% of the πN inelasticity this production channel had been included into the GiM calculations [1–9]. However due to the complexity of the problem the $2\pi N$ final state has been treated in a simplified way where only resonance decays into a 'generic' $2\pi N$ final state were allowed. This simplified treatment allowed to maintain two-body unitarity and reproduce partial wave cross sections extracted by Manley et al in [10]. In view of the large contribution to the πN inelasticity it is important to extend the calculations by treating three-body final states explicitly preserving three-body unitarity.

First, this approach would allow for the direct analysis of the $2\pi N$ experimental data. Since the corresponding Dalitz plots are found to be strongly non-uniform it is natural to assume that the main effect to the reaction comes from the resonance decays into isobar subchannels [10]. The most important contributions are expected to be from the intermediate σN, $\pi\Delta(1232)$, and ρN states. Analysis of the $\pi N \to 2\pi N$ reaction would therefore provide very important information about the resonance decay modes into different isobar final states. Presently lattice simulations [11, 12] and functional approaches [13] succeeded in calculation of the spectrum of QCD. Therefore unambiguous identification of the excited spectrum of baryons would provide an important link between theory and experiment. Similar to the constituent quark models [14, 15] the lattice QCD calculations demonstrate a much richer spectrum [11] of the non-strange sector of QCD than observed in scattering experiments so far. On the experimental side most of the non-strange baryonic states have been identified from the analysis of the elastic πN data [16–18]. As pointed out in [14] the signal of excited states with a small πN coupling could be suppressed in the elastic πN scattering. As a solution to this problem a series of photoproduction experiments has been done to accumulate enough data for study of the nucleon excitation spectra. However, the results from the photoproduction reactions are still controversial. While recent investigations of the photoproduction reactions presented by the BoGa group [19] reported indications for some new resonances not all of these states are found in other calculations [20]. This raises a question about independent confirmation for the existence of such states from the investigations of other reactions.

Because of the smallness of the electromagnetic couplings the largest contribution to the resonance self-energy comes from the hadronic decays. If the $N^* \to \pi N$ transition is small one can expect sizable resonance contribution into remaining hadronic decay channels. As

a result the effect from the resonance with a small πN coupling could still be significant in the inelastic pion-nucleon scattering: here the smallness of resonance coupling to the initial πN states could be compensated by the potentially large decay branching ratio to other different inelastic final states. Such a scenario is realized e.g. in the case of the well known $N^*(1535)$ state. While the effect from this resonance to the elastic πN scattering is only moderate at the level of total cross section its contribution to the $\pi N \to \eta N$ channel turns out to be dominant [7]. Since the $\pi N \to 2\pi N$ reaction could account for up to 50 % of the total πN inelasticity this channel becomes very important not only for the investigation of the properties of already known resonances but also for the search for the signals of possibly unresolved states.

Another important issue in studies of the $2\pi N$ channel is related to the possibility to investigate cascade transitions like $N^{*\prime} \to \pi N^* \to \pi\pi N$, where a massive state $N^{*\prime}$ decays via intermediate excited N^* or Δ^*. It is interesting to check whether such decay modes are responsible for the large decay width of higher lying mass states. So far only the $\pi N^*(1440)$ isobar channel has been considered in [10] in a partial wave analysis (PWA) of the $\pi N \to 2\pi N$ experimental data [10].

There are several complications in the coupled-channel analysis of $2 \to 3$ transitions. The first one is the difficulty to perform the partial-wave decomposition of the three-particle state. The second complication is related to the issue of three-body unitarity. For a full dynamical treatment of the $2 \to 3$ reaction the Faddeev equations have to be solved. This makes the whole problem quite difficult for practical implementations. Here we address both issues and present a coupled-channel approach for solving the $\pi N \to 2\pi N$ scattering problem in the isobar approximation. In this formulation the $(\pi/\pi\pi)N \to (\pi/\pi\pi)N$ coupled-channel equations are reduced to the two-body scattering equations for isobar production. Such a description accounts by construction for the full spectroscopic strength of intermediate channels and, in addition provides a considerable numerical simplification. Three-body unitarity leads to a relation between the imaginary part of the elastic scattering amplitude and the sum of the total elastic and inelastic cross sections by the well known optical theorem. Since in the isobar approximation the pions in the $\pi\pi N$ channel are produced from the isobar subchannels all contributions to the total $\pi N \to \pi\pi N$ cross section are driven by the isobar production. The optical theorem can be fulfilled if all discontinuities in isobar subchannels are taken into account. In the present work the three-body unitarity is maintained up to

interference term between the isobar subchannels.

As a first application of our model we apply the developed approach for the study of the $\pi^- p \to \pi^0\pi^0 n$ data in the first resonance energy region assuming the dominant S_{11} and P_{11} partial wave contributions in the σN and $\pi\Delta$ reaction subchannels. The main purpose of this paper is to introduce the model and demonstrate the feasibility of treating two-pion dynamics in the framework of a large-scale coupled channels approach. For this aim, we restrict the calculations to the $\pi^0\pi^0 n$ channel, taking advantage of the fact that only isoscalar two-pion and $\pi\Delta$ isobar channels are contributing to the process. We emphasize that this restriction is not a matter of principle but is only for the sake of a feasibility study. In particular, this means that at this stage we do not consider the ρN state but postpone its inclusion into the numerical scheme to a later stage. Naturally, the results presented in the following are most meaningful for the energy region of the $N^*(1440)$ Roper resonance.

The first resonance energy region is of particular interest because of the sizable effect from $N^*(1440)$. The dynamics of the Roper resonance turns out to be rich because of the two-pole structure reported in earlier studies [21, 22], (see [16, 23, 24] for the recent status of the problem.) The origin of the Roper resonance is also controversial. For example the calculations in the Jülich model explain this state as a dynamically generated pole due to the strong attraction in the σN subchannel. At the same time the Crystal Ball collaboration finds no evidence of strong t-channel sigma-meson production in their $\pi^0\pi^0$ data [25]. From the further analysis of the $\pi^0\pi^0$ production the effect of the sigma meson was found to be small [26]. On other hand the $pp \to pp\pi^0\pi^0$ scattering experiment by CELSIUS-WASA collaboration [27] finds the σN decay mode of the Roper resonance to be dominant.

The $2\pi N$ decay properties of the Roper resonance are also under discussion. The recent multichannel analysis from the Kent group [28] gives the branching ratios for the σN and $\pi\Delta(1232)$ decay modes $\mathrm{R}_{\sigma N}^{N(1440)} = 27 \pm 1\%$ and $\mathrm{R}_{\pi\Delta(1232)}^{N(1440)} = 6.8 \pm 0.8\%$, respectively. At the same time Anisovich et al [19] obtain a significantly larger decay fraction for the $\pi\Delta(1232)$ channel $\mathrm{R}_{\pi\Delta(1232)}^{N(1440)} = 21 \pm 8\%$ and somewhat smaller for the σN: $\mathrm{R}_{\sigma N}^{N(1440)} = 17 \pm 7\%$.

In view of these problems we perform an analysis of the Crystal Ball data [29] assuming dominant contributions from the S_{11} and P_{11} amplitudes in the isospin $I = \frac{1}{2}$ channel. Since the effect from $N^*(1520)$ is expected to be important above 1.46 GeV we have limited the present calculations up to $\sqrt{s}$ =1.46 GeV energy region. Using unitarity the contribution from $N^*(1520)$ to the total $2\pi N$ cross section could be estimated. The effect from the latter

state is thus can be taken into account for the error estimation of the extracted parameters of the $N^*(1440)$ resonance. The interaction kernel used in the scattering equation is calculated from the corresponding interaction Lagrangians. Though the effect from the background terms are found to be small, the t-channel pion exchange of the σ meson production turns out to be important close to threshold.

The σN decay fraction of $N^*(1440)$ is found to be dominant. The extracted value $R_{\sigma N} \approx 27\%$ is about two times larger than that of $\pi\Delta$: $R_{\pi\Delta} \approx 12\%$. The extracted partial waves of the isobar production are close to the single energy solutions(SES) from the analysis of Manley et al [10] except for the sign at the real part of the σN reaction amplitudes. The calculated S_{11} and P_{11} inelasticities demonstrate a good agreement with the results from the GWU group [16]. In the present study the Roper resonance is treated as a genuine pole. An alternative scenario would be to describe $N^*(1440)$ in terms of a dynamical pole. However, if such a pole is generated by the, e.g., t-channel exchange in the isobar production channel the angular dependence of the reaction amplitude could be different from the case with genuine pole. One may hope that the detailed analysis of the $2\pi N$ production channels could help to disentangle the different scenarios. The forthcoming measurements of the $\pi N \to 2\pi N$ reaction at HADES and JPARC facilities provide a new possibility to solve these long standing problems in the non-strange baryon spectroscopy.

The paper is organized as follows: in Section II we present a short overview of the partial wave analysis of the $\pi N \to 2\pi N$ reactions. The details of the Giessen Model (GiM) are presented in Section III. The impact of the isobar dynamics on the data analysis is presented in Section IV. The results of the calculations and the partial wave analysis are discussed in Section V.

II. OVERVIEW OF THE $\pi N \to 2\pi N$ REACTION

Here we present a short overview of the analyses of the $\pi N \to 2\pi N$ reaction made so far. Further details can be found in the papers cited in the present section. One of the most extensive studies of $2\pi N$ production in the resonance energy region has been made by Manley et al in [10]. There a partial wave analysis of the $\pi N \to 2\pi N$ experimental data was performed within the isobar approximation. The database consisted of old 241214 bubble chamber events in the energy region 1.320-1.93 GeV taken before 1984. No $\pi^0\pi^0 n$

data were available at the time. By binning the events into 22 energy bins and performing a sophisticated truncation scheme to reduce the number of independent amplitudes partial wave contributions were obtained for each isobar channel. The dependence on the energy of the isobar was neglected and neither two- or three-body unitary was explicitly maintained. The main result of the work [10] are single energy solutions (SES) extracted for each isobar channel in every energy bin. Since the dependence on isobar subenergy was neglected in [10] the derived solutions are simple functions of the c.m. energy.

In general the PWA of experimental data does not provide direct information about N* spectra: it only helps to disentangle contributions into the different partial wave amplitudes using conservation laws for total spin, parity and isospin. To investigate the reaction dynamics theoretical energy-dependent amplitudes should be defined. A specific parameterization of the scattering amplitude could be used to construct the scattering amplitudes. The non-resonant contributions can be parameterized in terms of smooth polynomial functions or by distant poles. The dynamical approaches are based on solving relativistic scattering equations to calculate the transition amplitudes. These calculations pursue the description of the scattering process in terms of mesons and baryons as the effective degrees of freedom of low-energy QCD. Since the interaction kernel is obtained from the given Lagrangian densities important constraints, e.g. chiral symmetry, can be also respected.

Since we describe the pseudoscalar vertices by derivative couplings [1, 3] the Giessen model accounts for a central requirement of chiral symmetry, at least at the minimal level of interaction vertices. In view of the large energy range covered by our analyses we have been using in the past a mesonic picture by explicitly using scalar and vector mesons as the relevant degrees of freedom rather than following the scheme of chiral perturbation theory and expressing those channels in terms of a perturbative multi-pion expansion. In this paper, we are making a first step towards a more detailed description of meson production on the nucleon by treating explicitly the two-pion resonance nature of a selected subset of the heavy mesons. We emphasize again that we are well aware of the limitations of such a restricted approach, primarily intended as a feasibilty study of two-pion production in the frame work of a coupled channels approach. Our approach is based on a field-theoretical Lagrangian formulation, fully accounting for Lorentz-invariance and the relevant internal symmetries.

The next step is to constrain the theoretical amplitudes to SES and fix the resonance parameters. Alternatively the calculated amplitudes could also be fitted directly to the data

without an PWA analysis of experimental observables as an intermediate step.

Several studies [28, 30, 31] have been made to extract the nucleon excitation spectra from the single-energy solutions (SES) derived in [10]. The KSU approach is based on multichannel parameterization of the scattering matrix in the form $S = (1 + iK)/(1 - iK)$ within K-matrix formalism [30] whereas the calculations [31] utilize CMB ansatz of Cutkosky et al [32]. While both approaches are able to maintain at least two-body unitarity their PWA amplitudes are fitted to the single energy solutions from [10] which are obtained by neglecting this constraint.

A combined analysis of the $\pi^0\pi^0 N$ production channel from the γp and $\pi^- p$ scattering has been presented in [33]. The authors do not use the SES from [10] but fit the calculated observables directly to the experimental data. One of the interesting conclusions made in [33] is that in photoproduction the background contributions to the $\pi^0\pi^0$ production are as large as the resonant one. Note that the analysis of the two-pion photoproduction data is more involved due to the complications related with the gauge invariance [34]. On the other hand the non-resonant terms play only a minor role in the $\pi^- p \to \pi^0\pi^0 n$ scattering [33]. As a result the latter reaction is better suited for an investigation of the properties of the Roper resonance [33]. The decay width of $N^*(1440)$ is found to be $\Gamma_{\sigma N}^{N(1440)} = 71 \pm 17$ MeV and $\Gamma_{\pi\Delta(1232)}^{N(1440)} = 59 \pm 15$ MeV which leads to the slightly larger σN decay fraction. The updated analysis [19] gives $\mathrm{R}_{\pi\Delta(1232)}^{N(1440)} = 21 \pm 8\,\%$ and $\mathrm{R}_{\sigma N}^{N(1440)} = 17 \pm 7\,\%$ which are different from [28].

Several dynamical approaches have been developed to investigate the $\pi N \to 2\pi N$ scattering. The Jülich model [35, 36] obtains the scattering amplitudes by solving the Lippmann-Schwinger equation where the two-pion production is treated in the isobar approximation. One of the interesting results obtained in Jülich model is that the Roper resonance could be represented by a dynamically generated pole due to the correlations in the σN subchannel. However no direct comparison of their calculations to the $\pi N \to \pi\pi N$ experimental data has been made so far [36].

An investigation of the properties of $N^*(1440)$ has been presented in [37] where the authors also applied the isobar approximation. A set of chiral constraints has been used to derive amplitudes for the $\pi N \to \pi\Delta(1232)$, σN transitions. The results of calculations are compared with the total experimental $\pi N \to 2\pi N$ cross sections and the Crystal Ball measurements of the $\pi^0\pi^0 n$ production. Both the $\pi\Delta(1232)$ and the σN decay modes of

$N^*(1440)$ are found to be important [37].

There are several studies of the $\pi N \to 2\pi N$ reaction within the chiral perturbation theory [38–41]. In general the chiral calculations in the heavy baryon limit demonstrate a nice agreement with experiment in the low energy region. One of the important results from the chiral calculations is that the effect from one loop diagrams is negligible [38]. By fixing low energy constants from the comparison with the $\pi^- p \to \pi^-\pi^+ n$ experimental data the predictions for the other charge transitions are given. Though the contributions from excited states are encoded into low energy constant (LEC's) the analytical structure of the scattering amplitude could be quite different from the case when resonance are explicitly included into calculations. Recent calculations including $\Delta(1232)$-isobar are presented in [42].

In addition several meson exchange models have also been used to attack the problem [43, 44]. The authors of [43] apply a tree-level parameterization to evaluate two-pion production. It is interesting that the authors do not use the Breit-Wigner parameterization but obtain the vertices and the propagators at the tree-level diagrams by solving dynamical equations. In addition to $N^*(1440)$ several additional states have also been included into the calculations. Close to threshold the findings of [43] demonstrate a nice agreement with experiment. These results also support a large contribution from the Roper resonance to the $\pi^- p \to \pi^+\pi^- n$ and $\pi^- p \to \pi^0\pi^0 n$ reactions which is in line with the conclusions of [33, 37]. Though the authors of [43] do not give their decay branching ratios for resonance decays, one might expect a sizable $\mathrm{N}^{\frac{1}{2}+}(1440) \to \sigma n$ decay fraction from the large $\mathrm{g}_{\sigma NN(1440)} \gg \mathrm{g}_{\pi\Delta(1232)N(1440)}$ coupling constant in [43].

Another dynamical approach to solve the coupled-channel problem for the two pion production is presented in [45, 46]. This approach is close in spirit to [36]. The model aims to go beyond the isobar approximation having both dispersive contributions and unitarity cuts under control.

Since the full calculations require large computation efforts only a limited amount of $\gamma/\pi N \to \pi\pi n$ experimental data has been analyzed, see [47, 48] and references therein. One of the complications reported in [45] is the appearance of the moving singularity in the scattering amplitude. Presently it is not clear whether the phenomena has a physical origin or is related to the treatment of the scattering problem in the Euclidean space.

III. COUPLED-CHANNEL UNITARY MODEL FOR $\pi N \to 2\pi N$ SCATTERING

A. The issue of unitarity

Unitarity is a one of the important key issues in the partial wave analysis. This constraint is maintained in a coupled-channel treatment of the scattering problem. The requirement that the sum of all transition probabilities should be 1 leads to the condition $SS^+ = 1$ for the scattering S-matrix. This gives

$$-i(T - T^+) = TT^+ \tag{1}$$

for the T-matrix in the operator form. On the amplitude level it leads to a relation between the imaginary part of the elastic scattering amplitude and the transition probability summed over all elastic and inelastic asymptotic channels

$$\mathrm{Im}T_{ii} = \sum_j T_{ij}T_{ij}^+ = \sum_j |T_{ij}|^2, \tag{2}$$

where indices i, j denote incoming and outgoing asymptotic final states, e.g. πN, $2\pi N$ etc, and their quantum numbers. The summation in Eq. (2) stands for summation over spin, isospin and integration over intermediate particle momenta. From the form of relation Eq. (2) follows that the scattering amplitude T is a matrix of dimension N×N where N is the number of all open channels and independent spin-isospin combinations.

For the sake of simplicity we consider here πN scattering below the $3\pi N$ threshold. Then only πN and $2\pi N$ final states are important on the right side of Eq. (2); the electromagnetic processes can be neglected. The quantity T_{ii} denotes a scattering amplitude for elastic transitions where all quantum numbers (including momenta) of the particles in the in-state are identical to those in the out-state. This can only take place for the elastic scattering at forward directions. Then, for the elastic πN scattering one can write $T_{ii} = T^{\mathrm{els.}}_{\pi N}(0)$, where $T^{\mathrm{els.}}_{\pi N}(0)$ is the πN elastic scattering amplitude for forward angles. Eq. (2) can be rewritten in the form of the optical theorem

$$\mathrm{Im}T^{\mathrm{els.}}_{\pi N}(0) = \frac{k^2}{4\pi}(\sigma_{\pi N\to\pi N} + \sigma_{\pi N\to 2\pi N}), \tag{3}$$

where k is a c.m. momentum of the initial πN state and $\sigma_{\pi N\to\pi N}$ and $\sigma_{\pi N\to 2\pi N}$ denote the total $\pi N \to \pi N$ and $\pi N \to 2\pi N$ cross sections respectively. For higher energies the

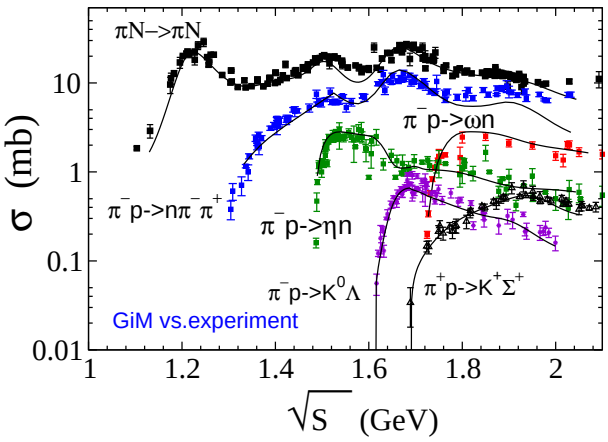

FIG. 1: (Color online) total cross sections for pion-induced reactions calculated in Giessen model [5–9] vs. experimental data.

right hand side of equation Eq. (3) can include contributions from other open channels. The importance of the optical theorem for the data analysis can be seen after the partial wave decomposition of Eq. (3):

$$\mathrm{Im}T^{JP}_{\pi N} = \frac{k^2}{4\pi}(\sigma^{JP}_{\pi N\to\pi N} + \sigma^{JP}_{\pi N\to 2\pi N}), \tag{4}$$

where the subscripts J and P stand for the total spin and the parity. As a consequence the imaginary part of the given elastic πN partial wave is a sum over all elastic and inelastic total partial wave cross sections. The results of GiM-calculations [5–9] are shown in Fig. 1. All reactions turn out to be linked via Eq. 3 and its PWA-version, Eq. (4). The largest inelastic contribution to the left-hand part of Eqs. (3,4) comes from the $\pi N \to 2\pi N$ reactions. Hence it is very important that the $2\pi N$ channel is included in the PWA for the baryon resonance analysis. In our earlier work the $2\pi N$ final state was treated as a 'generic' channel to control inelasticities associated with the $\pi N \to 2\pi N$ reaction, see [3, 4]. Here we discuss the extension of the model to incorporate the $2\pi N$ channel within the isobar approximation.

B. Giessen Model (GiM) for the $\pi N \to \pi N$, $2\pi N$ transitions

Though unitarity is a general property which is independent of the specific form of the scattering equation to be solved it is easier to consider the problem for the example of the Bethe-Salpeter equation in the ladder approximation. There are three amplitudes $T_{\pi N\to\pi N}$,

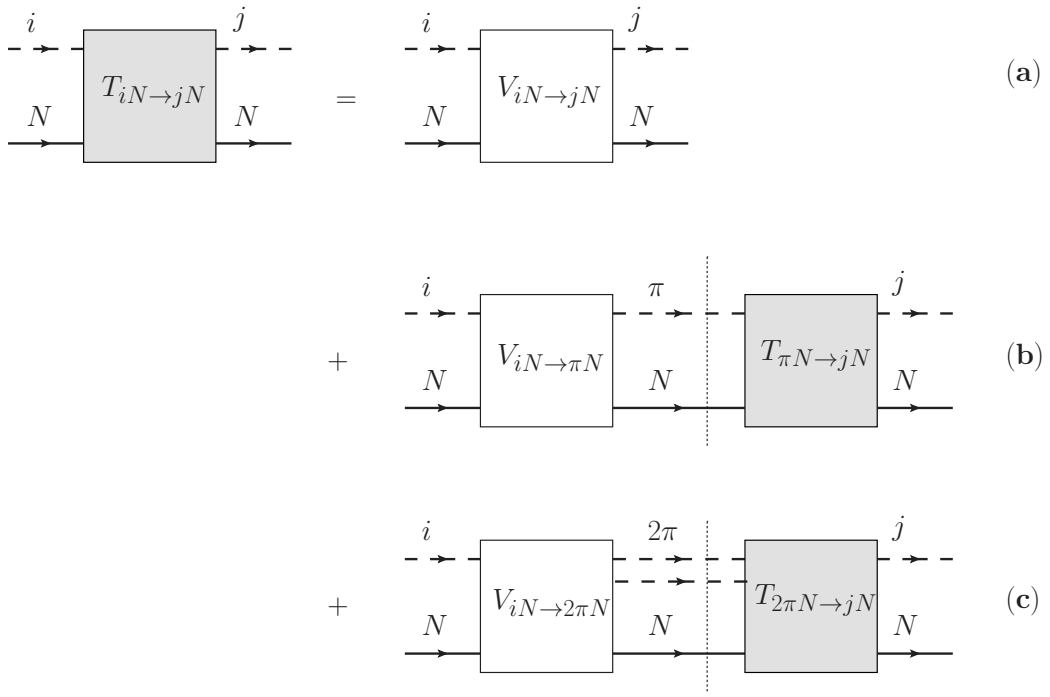

FIG. 2: Scattering equation for the process $iN \to jN$ where i, j=πN,$2\pi N$; $V_{iN\to jN}$ stands for the interaction kernel.

$T_{\pi N\to 2\pi N}$ and $T_{2\pi N\to 2\pi N}$ which are obtained by solving the system of scattering equations. The structure of these equations is represented diagrammatically in Fig. 2, where $V_{iN\to jN}$ denotes the interaction kernel. In order to fulfill the optical theorem, Eqs. (3,4), the πN and $2\pi N$ unitarity cuts have to be taken into account. The optical theorem for the $2 \to 2$ transitions has thoroughly been discussed in [3–5]. Here we concentrate on the last term in the scattering equation which contains the $2\pi N$ loop, see Fig. 2(c).

In the isobar approximation the main contribution to the $2\pi N$ final state comes from the decays of isobars. For, e.g., the $\pi^- p \to \pi^0\pi^0 n$ reaction at low energies the main effect is expected to be from the σN and $\pi\Delta(1232)$ subchannels. By taking care of the symmetrization of the $\pi^0\pi^0$ state the term (c) in Fig. 2 can be rewritten via isobar production amplitudes as demonstrated in Fig. 3. From the representation in Fig. 3 it follows that the problem of solving the equations depicted in Fig. 2 is reduced to the that of calculating the isobar production amplitudes

$$T_{\pi N\to\pi\Delta(1232)},\ T_{\pi N\to\sigma N}\ T_{\sigma N\to\sigma N}\ \text{etc.} \tag{5}$$

The σ-meson and $\Delta(1232)$-isobar are treated as unstable particles with masses of $m_\sigma^2 =$

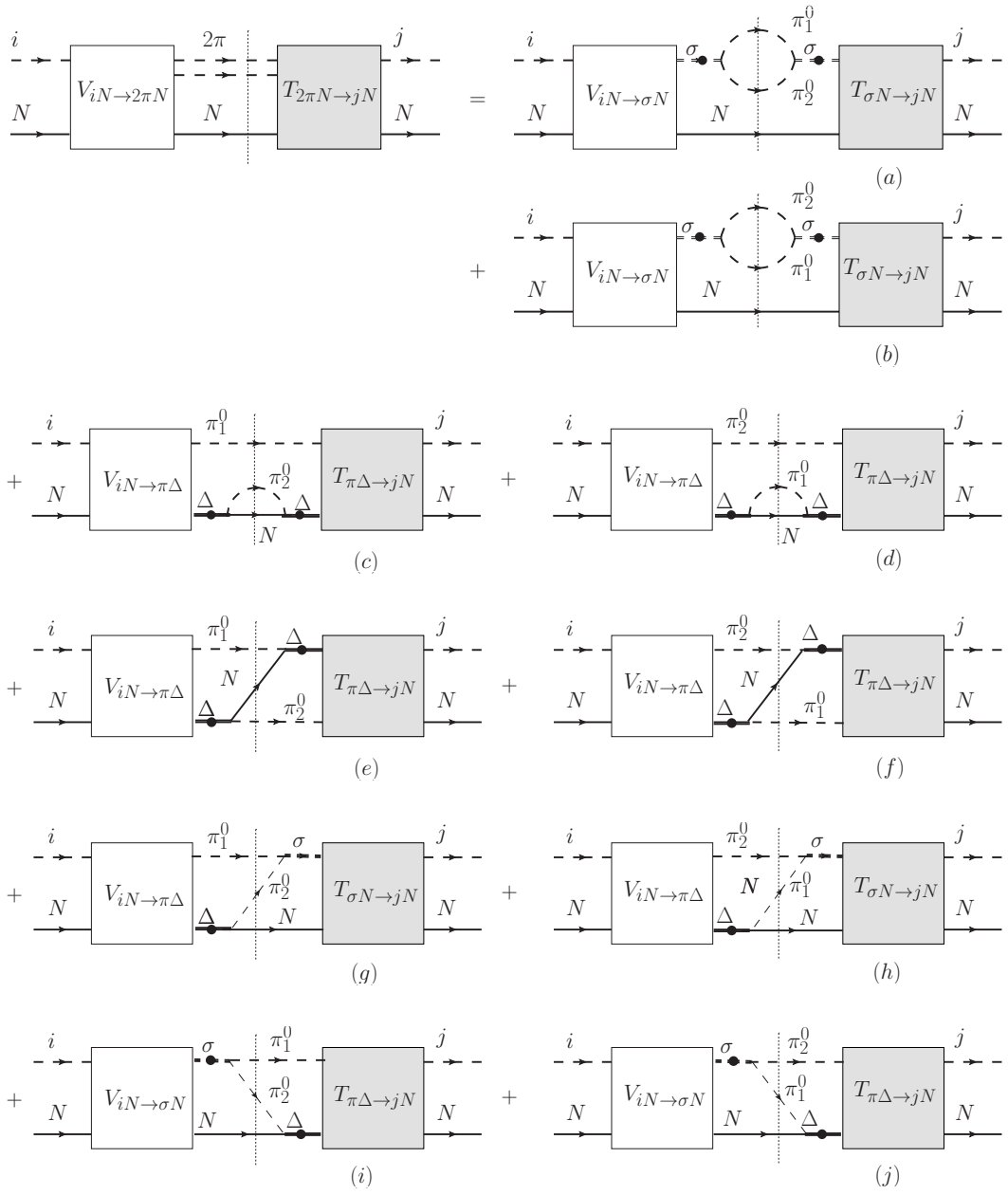

FIG. 3: Representation of the graphs depicted in Fig. 2 (c) in term of the isobar contributions.

$(q_{\pi_1^0}+q_{\pi_2^0})^2$ and $m_\Delta^2=(q_{\pi_1^0}+p'_N)^2$ respectively. Here $q_{\pi_1^0}$, $q_{\pi_2^0}$, and ${p'_N}^2$ are final four-momenta of the final pions and the nucleon. The $\pi^- p\to\pi^0\pi^0 n$ transition rate can be obtained from the isobar production amplitudes as shown in Fig. 4. Assuming that the properties of isobars are known the problem of calculation of the $\pi N\to\pi\pi N$ transitions rates can be reduced to the problem of evaluation of the isobar production amplitudes Eqs. (5).

To simplify the discussion we first consider the situation where the two-pion production

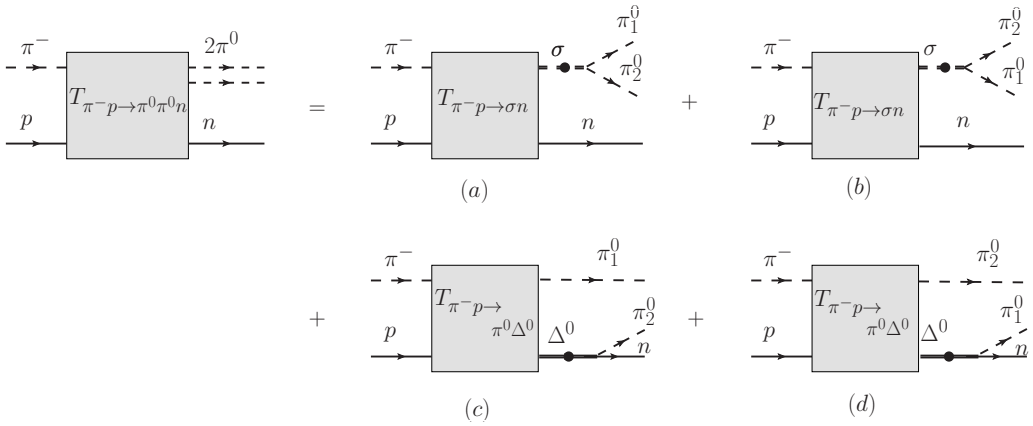

FIG. 4: The $\pi^- p \to \pi^0\pi^0$ reaction expressed via the isobar production amplitudes.

exclusively proceeds via the σN subchannel. In this case only the subprocesses depicted in Fig. 3(a) and Fig. 3(b) contribute to the scattering equation presented in Fig. 2. The two-pion loop in the Fig. 3(a,b) stands for the rescattering process in the isoscalar subchannel accounting for correlations due to the $\pi\pi$-interaction. In the ladder approximation the equation for the σ-meson propagator reads

$$G_\sigma(q_\sigma) = G^0_\sigma(q_\sigma) + \int \frac{d^4k}{(2\pi)^4} G^0_\sigma(q_\sigma) V_{\sigma\to 2\pi}(q_\sigma, k) G_{2\pi}(q_\sigma, k) V_{\sigma\to 2\pi}(q_\sigma, k) G_\sigma(q_\sigma), \tag{6}$$

where $V_{\sigma\to 2\pi}$ is the $\sigma\pi\pi$ decay vertex, $G^0_\sigma(q_\sigma) = (q^2_\sigma - m^2_{\sigma_0} + i0)^{-1}$, and $G_{2\pi}$ denotes the two-pion propagators. To keep the problem as simple as possible the solution of the σ-meson propagator, Eq. (6), is obtained in the $K-$ matrix approximation [49] which allows the propagator to be expressed in the form

$$G_\sigma(p_\sigma) = \frac{1}{q^2_\sigma - m^2_{\sigma_0} - i\mathrm{Im}\Sigma_\sigma(q_\sigma)}, \tag{7}$$

where only the imaginary part of the σ-meson self-energy $\mathrm{Im}\Sigma_\sigma$ is taken into account. In the present approximation the σ-meson can be understood as an unstable particle with the quantum numbers $\mathrm{J^{IP}} = 0^{0+}$ and the mass of $m^2_\sigma = (q_{\pi_1} + q_{\pi_2})^2$. The $\sigma\pi\pi$-coupling is given in Appendix E.

The scattering equation for the isobar amplitudes can be written in the form

$$\begin{aligned}\langle f|T(k',k)|i\rangle = \langle f|V(k',k)|i\rangle &+ \int \frac{d^4q'}{(2\pi)^4} \langle f|T(k',q')G_{\pi N}(q')V(q',k)|i\rangle \\ &+ \int \frac{d^4q}{(2\pi)^4} \langle f|T(k',q)G_{\sigma N}(q)V(q,k)|i\rangle\,,\end{aligned} \tag{8}$$

where i, f denotes initial and final states $i, f = \pi N, \sigma N$. $G_{\pi N}(q')$ and $G_{\sigma N}(q)$ stands for the πN and σN propagators respectively. k and k' stand for the c.m. momenta of the incoming and outgoing meson. Solving Eq. (8) turns out to be technically complicated. A considerable numerical simplification is obtained by the $K-$matrix approximation which consists in neglecting the dispersive part in Eq. (8). The technique and the relevance of this approximation was thoroughly discussed e.g. in [49, 50]. This approximation also allows to solve the scattering equation in Minkowsky space. The transformation of the first term in the right part of Eq. (8) is presented [1, 3, 49, 50], here we only consider the second term in Eq. (8). Its contribution corresponds to graphs displayed in Fig. 3(a,b) and can be written in the form

$$\int \frac{dq_0\, d^3q}{(2\pi)^4} < f|T(k',q)\, \frac{\not{p} - \not{q} + m_N}{(p-q)^2 - m_N^2 + i0}\, \frac{1}{(q+p)^2 - m_\sigma^2 + i\mathrm{Im}\Sigma_\sigma\left((p+q)^2\right)} \cdot V(q,k)|i > \quad (9)$$

with $p = (\sqrt{s}/2, 0, 0, 0)$ and s being the Mandelstam variable. The discontinuity of the fermion propagator Feucan easily be taken into account [3, 49] which reduces Eq. (9) to

$$\int \frac{dq_0\, q\, d\Omega_q}{2(2\pi)^3} \sum_\xi T_{f,\sigma N}(k',q) \frac{1}{(q+p)^2 - m_\sigma^2 + i\mathrm{Im}\Sigma_\sigma\left((p+q)^2\right)} V_{\sigma N,i}(q,k). \quad (10)$$

where ξ denotes all quantum numbers of the intermediate particles states, $q = \sqrt{(\sqrt{s}/2 - q_0)^2 - m_N^2}$ is a c.m. momentum of σN subsystem. The sigma meson propagator can be rewritten in the form

$$\frac{1}{\mu^2 - m_\sigma^2 + i\mathrm{Im}\Sigma_\sigma(\mu^2)} = \frac{(\mu^2 - m_\sigma^2)}{(\mu^2 - m_\sigma^2)^2 + (\mathrm{Im}\Sigma_\sigma(\mu^2))^2} - \mathrm{i}\frac{\mathrm{Im}\Sigma_\sigma(\mu^2)}{(\mu^2 - m_\sigma^2)^2 + (\mathrm{Im}\Sigma_\sigma(\mu^2))^2},$$

where $\mu^2 = (p+q)^2 = 2q_0\sqrt{s}$. The first term gives rise to the dispersive corrections and is neglected here. Substituting the second term into Eq. (10) and replacing the integration variable $q_0 \to \mu_\sigma^2\sqrt{s}$ one gets

$$-\,\mathrm{i}\int \frac{d\mu_\sigma^2}{4\sqrt{s}} \frac{q\, d\Omega_q}{(2\pi)^3} \sum_\xi T_{f,\sigma N}(k',q) \frac{\mathrm{Im}\Sigma_\sigma(\mu_\sigma^2)}{(\mu_\sigma^2 - m_\sigma^2)^2 + (\mathrm{Im}\Sigma_\sigma(\mu_\sigma^2))^2} V_{\sigma N,i}(q,k). \quad (11)$$

By defining the spectral function of the σ-meson in the form

$$A_\sigma(\mu_\sigma^2) = \frac{1}{\pi} \frac{\mathrm{Im}\Sigma_\sigma(\mu_\sigma^2)}{(\mu_\sigma^2 - m_\sigma^2)^2 + (\mathrm{Im}\Sigma_\sigma(\mu_\sigma^2))^2} \quad (12)$$

one can rewrite Eq. (11) as follows

$$-\,\mathrm{i}\int \frac{q\, d\Omega_q}{8\sqrt{s}(2\pi)^2} \int_{4m_\pi^2}^{\sqrt{s}-m_N} d\mu_\sigma^2 A_\sigma(\mu_\sigma^2) \sum_\xi T_{f,\sigma N}(k',q) V_{\sigma N,i}(q,k). \quad (13)$$

Up to the additional integral over $d\mu_\sigma^2 A_\sigma(\mu^2)$ the quantity in Eq. (13) looks very similar to the rescattering in the two-body channel within the K-matrix approximation to BSE. Using the partial wave decomposition Appendix C the integral over $d\Omega_q$ can be calculated analytically. Then Eq. (8) reduces to the equations for the partial wave scattering amplitudes in the closed form:

$$T^{JP}_{f\,i}(\sqrt{s}) = K^{JP}_{f\,i}(\sqrt{s}) + \mathrm{i}\sum_j \int_{4m_\pi^2}^{\sqrt{s}-m_N} d\mu_j^2 A_j(\mu_j^2) T^{JP}_{f\,j} K^{JP}_{j\,i} \tag{14}$$

where $K = V$, $f, i, j = \pi$, σ and $A_\pi(\mu_\pi^2) = \delta(\mu_\pi^2 - m_\pi^2)$ and $A_\sigma(\mu_\sigma^2)$ is defined in Eq. (12). Since the two-pion discontinuities are taken into account the three-body unitarity in the form of the optical theorem of Eqs. (3,4) is strictly fulfilled, see Appendix A.

As a next step we consider the $\pi\Delta(1232)$ contribution to the two-pion production. The full $\pi^- p \to \pi^0\pi^0 n$ transition amplitude corresponds to the graphs (c) and (d) in Fig. 4. It can be written as a sum $T_{\pi^- p\to\pi^0\pi^0 n} = T^c + T^d$. The second term appears because of the symmetrization of the $\pi^0\pi^0$ final state. While in the case of σN the effect of the symmetrization is trivial in the case of $\pi^0\pi^0 N$ production via $\pi\Delta(1232)$ it leads to complications because the isobar momentum in the diagrams (c) and (d) of Fig. 4 is different. Then the two-pion production cross section is defined by the integral over three body phase space with the production probability

$$|T_{\pi^- p\to\pi^0\pi^0 n}|^2 = |T^c|^2 + |T^d|^2 + T^{cd}. \tag{15}$$

T^{cd} is a non-vanishing interference term due the symmetrization of the $\pi^0\pi^0$ final state. When only (c) and (d) terms in Fig. 3 are included into the scattering equation the three-body unitarity is fulfilled up to the interference T^{cd} term. This can be demonstrated in a similar way as discussed in Appendix A. To take into account the effect of this interference the contributions from the (e) and (f) terms in Fig. 3 should also be included into scattering equation. If both the σN and $\pi\Delta(1232)$ isobar channels contribute to the reaction it is also necessary to include contributions from the diagrams shown in Fig. 3(g-j). These terms correspond to the interference between amplitudes of the two-pion production via the σN and $\pi\Delta(1232)$ isobars. The contributions from the diagrams (e)-(j) cannot be reduced to the simple integral form of Eq. (14) but contain additional integration over kinematical variables. Since the data analysis requires a large number of iterations the evaluations of these amplitudes becomes numericaly very expensive. In the present study we neglect these

contributions keeping only contributions from the diagrams (a)-(d) in Fig. 3. Then the scattering equation of the isobar production becomes

$$T^{JP}_{fi}(\sqrt{s}) = K^{JP}_{fi}(\sqrt{s}) + \mathrm{i}\sum_j \int_{\mu^2_{\min}}^{\mu^2_{\max}} d\mu_j^2 A_j(\mu^2) T^{JP}_{fj} K^{JP}_{ji}, \tag{16}$$

where the spectral function of the $\Delta(1232)$-isobar is given by

$$A^i_\Delta(\mu^2_\Delta) = \frac{1}{\pi}\frac{\mathrm{Im}\Sigma^i_\Delta(\mu^2_\Delta)}{(\mu^2_\Delta - m^2_\Delta)^2 + (\mathrm{Im}\Sigma_\Delta(\mu^2_\Delta))^2}, \tag{17}$$

and $i = \frac{3}{2}, \frac{1}{2}$ denotes the spin projections of propagating the $\Delta(1232)$, and $\mathrm{Im}\Sigma_\Delta(\mu^2_\Delta) = \mathrm{Im}\Sigma^{\frac{1}{2}}_\Delta(\mu^2_\Delta) + \mathrm{Im}\Sigma^{\frac{3}{2}}_\Delta(\mu^2_\Delta)$. The three-body unitarity in form of the optical theorem of Eq. (3) is therefore fulfilled up to interference between different isobar production channels:

$$\mathrm{Im}T^{\mathrm{els.}}_{\pi N}(0) = \frac{k^2}{4\pi}(\sigma_{\pi N\to\pi N} + \sigma^{\mathrm{incohr}}_{\pi N\to 2\pi N}). \tag{18}$$

Here the total two-pion production cross section $\sigma^{\mathrm{incohr}}_{\pi N\to 2\pi N}$ is calculated neglecting interference between $\sigma N \leftrightarrow \pi\Delta(1232)$ and $\pi\Delta(1232) \leftrightarrow \pi\Delta(1232)$ channels, see Appendix B. The cross section $\sigma^{\mathrm{cohr}}_{\pi N\to 2\pi N}$ is evaluated taking the above terms into account. The size of the interference between the isobar contributions can then be estimated by comparing $\sigma^{\mathrm{incohr}}_{\pi N\to 2\pi N}$ and $\sigma^{\mathrm{cohr}}_{\pi N\to 2\pi N}$. In the present calculations the contribution from the $\pi\Delta(1232) \leftrightarrow \pi\Delta(1232)$ interference is found to be very small and comparable to the overall 1% accuracy of the calculations. A somewhat larger effect is observed for the $\sigma N \leftrightarrow \pi\Delta(1232)$ interference. However its contribution does not exceed the few percent level. In Section V we present results of calculation for the right and the left parts of Eq. (18) and compare the difference between $\sigma^{\mathrm{incohr}}_{\pi N\to 2\pi N}$ and $\sigma^{\mathrm{cohr}}_{\pi N\to 2\pi N}$. Note that the difference $(\sigma^{\mathrm{incohr}}_{\pi N\to 2\pi N} - \sigma^{\mathrm{cohr}}_{\pi N\to 2\pi N})$ is not directly equal to the sum of contributions from diagrams (e)-(j) in Fig. 3; the scattering equation should be re-iterated once the (e)-(j) diagrams are taken into account. However $(\sigma^{\mathrm{incohr}}_{\pi N\to 2\pi N} - \sigma^{\mathrm{cohr}}_{\pi N\to 2\pi N})$ can be used to estimate the size of such contributions which are found to be small in the present study. The magnitude of this difference also indicates the size of the violation of the constraint Eq. (4). We discuss this isssue in Section V D.

Note that the $\sigma N \leftrightarrow \pi\Delta(1232)$ interference is still important in the calculation of, e.g., the angular distributions. However this effect is small at the level of the total cross section, see discussion in Section V.

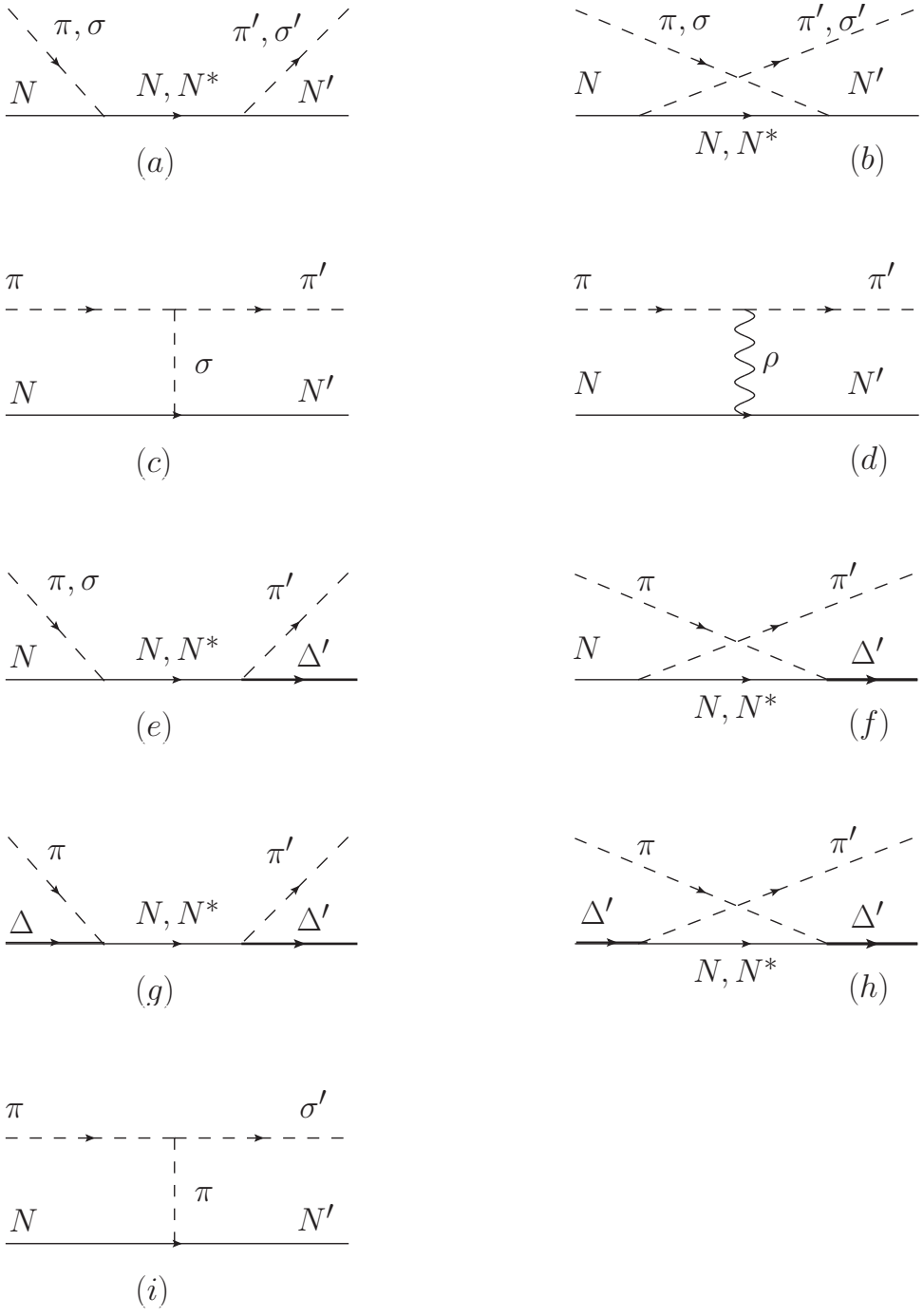

FIG. 5: Tree-level diagram contributions to the interaction kernel of the scattering equation.

C. Interaction kernel

To solve the scattering equation, Eq. (16), the interaction kernel must be specified. It is constructed as a sum of contributions from the tree-level diagrams shown in Fig. 5. For the

$(\pi/\sigma)N \to (\pi/\sigma)N$ scattering the diagram in Fig. 5(a) corresponds to the nucleon Born term and the resonances contributions. In the present study we concentrate on $I = \frac{1}{2}$ only and this include $N^*(1535)$ and $N^*(1440)$ states. The additional graph in Fig. 5(i) is responsible for the non-pole part in the σN subchannel. The driving terms for the $(\pi/\sigma)N \to \pi\Delta(1232)$ and $\pi\Delta(1232) \to \pi\Delta(1232)$ reactions are constructed from the s- and u-exchanges processes displayed in Fig. 5(e-h) with the ground state or excited nucleon in the intermediate state.

From the point of view of the $\pi N \to \pi\pi N$ transitions the processes (a) and (e) in Fig. 5 with the unstable baryon in the intermadiate state are resonant ones. The non-resonant term is described by the (b)-(d), (f), and (i) graphs in the same figure. The corresponding Lagrangian densities are given in Appendix E. Each vertex in dressed by the formfactor (e.g. for s-channel exchange)

$$F(q^2) = \frac{\Lambda^4}{\Lambda^4 + (q^2 - m^2)^2}, \tag{19}$$

where q^2 is the square of the four-momentum of exchange particle and m is its mass. To reduce the number of free parameters we use the same cutoff for all resonance decay channels $\Lambda_{N^*} = 1.95$ GeV. The cutoff at the nucleon vertex has been chosen to be $\Lambda_N = 0.95$ GeV. For the $t-$channel meson exchange we use Λ_t=1.54 GeV.

The coupling constants used in the calculations are listed in Table I. The values of the coupling constants $g_{\pi NN} = 12.8$ and $g_{\rho\pi\pi} = 6.02$ are the same as in our previous calculations [3–9]. The sign at $g_{\pi\Delta N}$ and its values are also taken in accordance with the results from [3–9]. The $g_{\rho NN}$, $\kappa_{\rho NN}$, and $g_{\sigma NN}$ coupling constants were allowed to be varied during fit. The $g_{\sigma\pi\pi}$ constant was fixed from the requirement to reproduce the σ-meson decay properties listed in PDG. With $g_{\sigma NN} = 3.25$ and $m_\sigma = 0.650\,\mathrm{GeV}$ the pole position $z_0 = (0.47 - 0.19\,\mathrm{i})$ GeV of the sigma meson is well reproduced [20]. We also obtain $z_0 = (1.210 - 0.5\,\mathrm{i})$ GeV for the pole position of $\Delta(1232)$. Since the isobar parameters could be subjected to small uncertainties we also allowed for small variation of $g_{\pi N\Delta}$ and $g_{\sigma\pi\pi}$ within a few percent during calculations. This allows for a small variation of background contributions in the $\pi N \to \pi\pi N$ reaction.

The resonance couplings to the $N^* \to \pi N$, σN, $\pi\Delta(1232)$ final state are constrained by the direct comparison of the calculated amplitudes to the experimental data. These parameters are discussed in Section V and Appedix E .

Within the isobar approximation the contribution from the nucleon Born term is ne-

g	value	g	value	g	value	g	value
$g_{\pi NN}$	12.8	$g_{\sigma NN}$	4.25	$g_{\rho NN}$	-0.69	$\kappa_{\rho NN}$	5.99
$g_{\sigma\pi\pi}$	3.25	$g_{\rho\pi\pi}$	6.02	$g_{\pi\Delta N}$	-2.2		

TABLE I: Nucleon and t-channel couplings. First line: C-calculations Second line: S-calculations.

glected. Here pions are produced from the nucleon intermediate state without forming an isobar. These terms can be regarded as a 'non-resonant background' to the $2\pi N$ production. Since the nucleon pole lies below the $2\pi N$ threshold no strong effect is expected from this transition. At the same time the nucleon Born term also gives rise to the process

$$\pi N \overset{N(938)}{\to} \pi\Delta(1232) \overset{\Delta\to\pi N}{\longrightarrow} \pi\pi N. \tag{20}$$

Because of the $\Delta(1232)$-isobar dynamics the effect from the 'non-resonant' term (20) is expected to be much larger than in the process without forming an isobar.

Our ansatz is also supported by the measurements in [26] where the mass distributions close to threshold are shifted to the higher invariant pion masses which is identified with the effect of σ-meson spectral function, see discussion in Section V.

IV. ISOBAR CONTRIBUTIONS TO THE $\pi N \to \pi^0\pi^0 N$ REACTION

In this section we discuss the impact of various observables on the partial-wave analysis. For unpolarized measurements the full information about the reaction dynamics is encoded into 4-fold differential cross sections, see e.g. Eq. (B5). In practice however the experiment often provides only a limited set of observables such as angular or mass distributions. This raises the question how different reaction channels can be extracted from experimental data. Hence it is an important issue to disentangle different decay modes of the same resonance.

In [26] measurements of the differential cross sections as a function of the nucleon scattering angle have been reported. The contributions from the σN and $\pi\Delta(1232)$ isobar channels to this observable are shown in Fig. 6 at the fixed energy $\sqrt{s} = 1.4$ GeV. The calculation is done assuming only a $J^P = \frac{1}{2}^+$-wave contribution to the production mechanism. Though the angular distribution is known to be very important for the partial wave analysis the

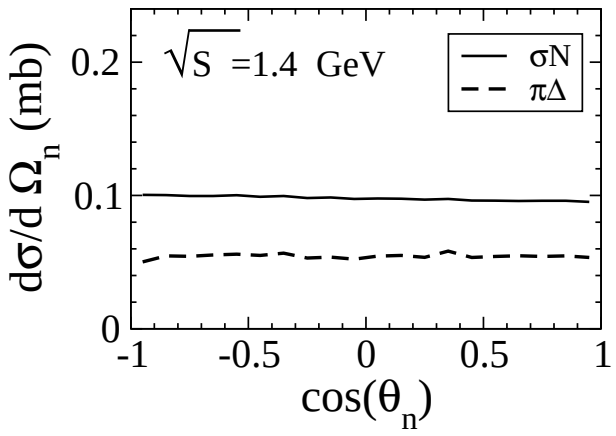

FIG. 6: Reaction $\pi^- p \to \pi^0\pi^0 n$: differential cross section as a function of the nucleon scattering angle. Solid line: effect of the $N^*(1440)$ resonance decay into the σN subchannel, dashed line: $N^*(1440)$ decay into the $\pi\Delta(1232)$ final state.

separation between the $\pi\Delta(1232)$ and σN subchannels turns out to be difficult. Both distributions are only weakly dependent on the nucleon scattering angle which indicates that each isobar subchannel is produced in the $J = \frac{1}{2}$ partial wave. However, any further separation between σN and $\pi\Delta(1232)$ subchannels is hardly possible.

On the other hand a great part of the information on the reaction dynamics in encoded in the experimental mass distributions. We first discuss the influence of the σ-meson spectral function on the results of the data analysis. This quantity appears explicitly in the scattering equation Eq. (16) and implicitly in the squared modulus of the $\pi\pi$ production amplitude in form of the product of the propagator and the decay vertex of the isobar, see Fig. (4) (a,b) and discussion in Appendix B.

First, it leads to an additional dependence of the production amplitude on the isobar mass. This is different to, e.g., the parameterization used in work of Manley et al [10] where single energy solutions are assumed to be functions only of the c.m. energy. The dependence on the isobar mass for the $\pi N \to \sigma N$ production amplitude is demonstrated in Fig. 7. The isobar production amplitude has a maximum at $m^2_{\sigma,\min} = 4m^2_\pi$ and vanishes for maximal values of $m^2_{\sigma,\max} = (\sqrt{s} - m_N)^2$. The latter effect would correspond to the σN reaction threshold if the σ-meson were a stable particle with mass of $m_{\sigma,\max}$. The spectral function demonstrates the opposite behavior: for the energy at hand $\sqrt{s} = 1.4$ GeV it is maximal for the maximal allowed invariant σ-meson mass and vanishes at $m^2_{\sigma,\min}$. The contribution from

the σN isobar channel to the two-pion production cross section is defined by the product of the modulus squared of the reaction amplitude and the σ-meson spectral function. This quantity is shown in Fig. 7 by the solid line. It demonstrates a rapid variation as a function of the σ-meson mass with the maximum lying in the interval $[m^2_{\sigma,\min}, m^2_{\sigma,max}]$. The position of the maximum is defined by the spectral function of the σ-meson, the c.m. energy $\sqrt{s}$, and the dynamics in the σN channel. For the energies at hand the resulting distribution is shifted to higher masses. A similar behavior is also seen in the experimental mass distributions close to the $2\pi N$ threshold. This allows to draw a conclusion on the important contributions from the σN subchannel to the $\pi^0\pi^0 n$ final state, as discussed below.

The analysis of the mass distribution $\mathrm{d}\sigma/\mathrm{d}m^2_{\pi^0\pi^0}$ for the pions produced from the $\pi\Delta(1232)$ isobar subchannel turns out to be more complicated. For the sake of simplicity we neglect for the moment the effect of the symmetrization for the two-pion final state. Let the first pion be produced in the $\pi N \to \pi\Delta(1232)$ transition and the second one in the $\Delta(1232)$ isobar decay. The invariant mass $m^2_{\pi^0\pi^0}$ is a function of the angle between the two pions. In the c.m. of initial particles the momentum of the first pion is opposite to the momentum of the $\Delta(1232)$-isobar. Hence the angular dependence between the two pions can be translated into the dependence on the angle between the second pion and the direction of the isobar momentum. The latter is defined by the spin structure of the decay vertex. In Fig. 8 the $\mathrm{d}\sigma/\mathrm{d}m^2_{\pi^0\pi^0}$ mass distribution is shown for pions coming from the $\pi\Delta(1232)$ subchannel which is produced in the $J^P = \frac{1}{2}^+$-wave. Therefore, only $\lambda_\Delta = \pm\frac{1}{2}$ helicity combinations contribute at the $\Delta \to \pi N$ decay vertex. For the decay at rest the transition probability behaves as

$$(1 + 3\cos^2\theta_\pi) \tag{21}$$

where θ_π is the angle between the momentum of the final pion and the direction of the isobar momentum. Eq. (21) exhibits a symmetric distribution with two maxima at $\theta_\pi = 0, \pi$. In the center of mass sytem of the initial πN particles the produced $\Delta(1232)$ isobar has a non-vanishing momentum. Therefore the dependence Eq. (21) becomes more complicated when the decay of the isobar is considered in the full three-body kinematics taking into account the effect of the symmetrization of the $\pi^0\pi^0$ states. However, even in this case the two maxima structure is clearly visible in the mass spectra shown in Fig. 8. A similar behavior is also found in the calculations of [37, 51].

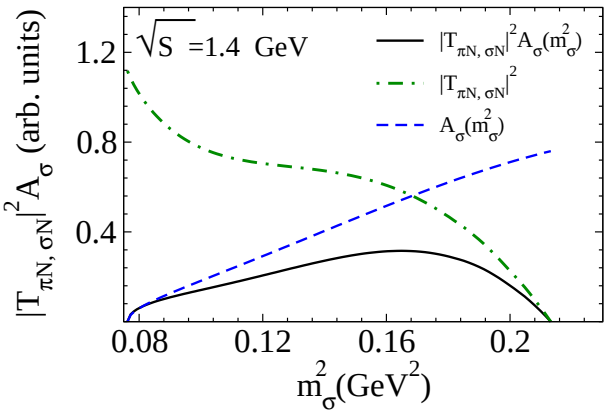

FIG. 7: (Color online) dash-dotted line: modulus of the average production amplitude squared $|T_{\pi N,\sigma N}|^2$ as a function of the invariant isobar mass $m_\sigma^2 = (q_1 + q_2)^2$, where q_1 and q_2 are pion momenta; dashed line: spectral function of the sigma meson $A_\sigma(m_\sigma^2)$ as a function m_σ^2. Solid line: $|T_{\pi N,\sigma N}|^2 A_\sigma(m_\sigma^2)$. All quantities are normalized by the arbitrary factors to put them together on the same figure.

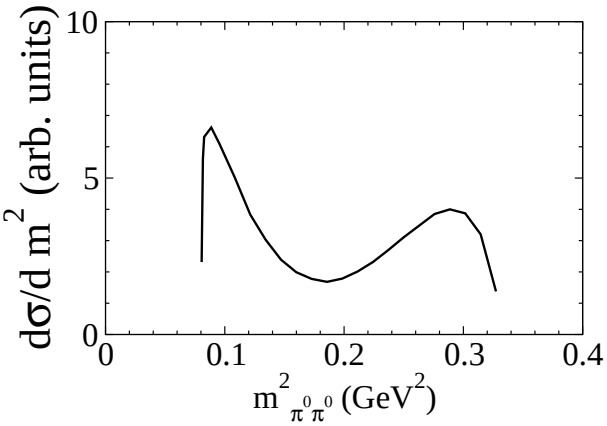

FIG. 8: Invariant mass distribution of the $\pi^0\pi^0 n$ system produced via $\pi\Delta(1232)$ subchannel in the P_{11} partial wave.

Comparison of the $\mathrm{d}\sigma/\mathrm{d}m^2_{\pi^0\pi^0}$ mass distributions for the σN and $\pi\Delta(1232)$ subchannels in Fig. 7, and Fig. 8 demonstrates very different mass dependencies for the isobar subchannels produced in the same partial wave. Hence the analysis of this observable becomes crucial for the identification of the resonance decay in the various isobar subchannels.

A. Non-resonant contributions into the $\pi N \to \pi^0\pi^0$ reaction

The non-resonant part of the interaction kernel consists of the s- and u-channel nucleon Born terms and the t- channel pion exchange for the $\pi N \to \sigma N$ transition, see diagram (i) in Fig. 5. Since the $g_{\pi NN}$, $g_{\sigma\pi\pi}$, and $g_{\pi N\Delta}$ couplings are fixed (see Section III C) the size of these contributions can be easily estimated. The result of the calculations without formfactors at the interaction vertices is shown in Fig. 9 vs. the data from [26]. At low energies the t-channel pion exchange gives rise to the s-wave scattering and the final σN system is produced in the $J = \frac{1}{2}$ state. Therefore the differential cross section demonstrates only a very weak angular dependence. We conclude that the t-channel pion exchange is responsible for the description of the $\pi^0\pi^0 n$ data close to threshold. However this mechanism starts to underestimate the data at energies above 1.3 GeV where the excitation of the Roper resonance is expected. With increasing c.m. energy the t-channel exchange starts to give rise to higher partial waves. This enhances the calculated cross section at forward angles as seen in the right panel of Fig. 9. Note that the overall effect from pion exchange is found to be smaller than would be expected from the large $g_{\sigma\pi\pi}$ and $g_{\pi N\Delta}$ coupling constants. This is because the σN contribution to the differential cross section at hand can be represented as an integral of the modulus squared of the isobar production amplitude multiplied by the σ-meson spectral function, $|T_{\pi N\to\sigma N}|^2 A_\sigma$, over the invariant two-pion mass $m^2_{\pi^0\pi^0} = m^2_\sigma$ (see discussion in Appendix A). The dependence of $|T_{\pi N\to\sigma N}|^2$ and A_σ on m^2_σ were shown in Fig. 7. These quantities demonstrate an opposite behavior at higher invariant masses: while the spectral function rises the isobar production amplitude declines. This reduces the total effect which is shown by the solid line in Fig. 7. We conclude that realistic calculations should account for the dependence on the dynamical isobar mass both in the production amplitude and for the propagation and decay of the σ-meson.

The nucleon Born term also gives an important contribution to the $\pi^0\pi^0 n$ production through the coupling to the $\pi\Delta(1232)$ isobar channel. However, close to the $2\pi N$ threshold its effect turns out to be smaller than that of the pion-exchange; the same conclusion has been drawn in [37]. Note that the non-resonant contributions discussed above are fixed up to a cutoff at the interaction vertex which has to be constrained during the fit.

Another source of the non-pole components in the interaction kernel for isobar production comes from the nucleon coupling to σN, see diagrams (a) and (b) in Fig. 5. The $g_{\sigma NN}$

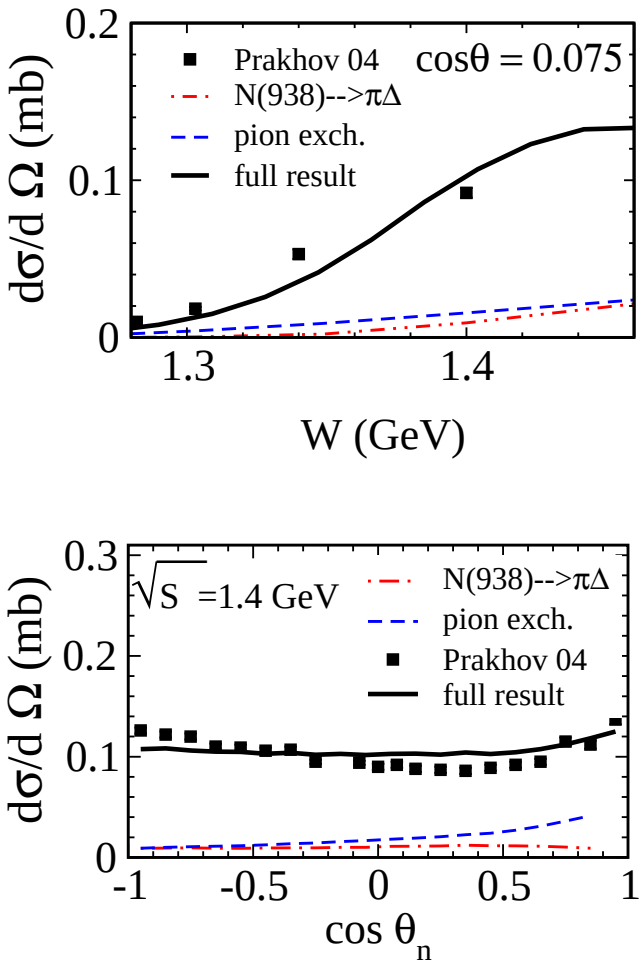

FIG. 9: (Color online) non resonant contribution to the $\pi^0\pi^0 n$ production as a function of the c.m. energy (upper panel) and the nucleon scattering angle (lower panel). Dashed line: t-channel pion exchange. Dash-dotted line: Nucleon s-channel contribution to the $\pi\Delta(1232)$ isobar channel. Solid line: full model. The experimental data denoted by Prakhov 04, are taken from [26].

coupling constant and the cutoff are fixed during the fit. However, the same vertex together with the ρ-meson exchange is also responsible for the description of the S_{11}- wave amplitude of the πN elastic scattering at low energies. The corresponding diagrams are shown in Fig. 5(c,d). This provides an additional constraint on the size of $g_{\sigma NN}$. The obtained value is given in Table I.

The calculated nucleon Born term contribution to the σN production, see diagrams Fig. 5(a,b), turns out to be significantly smaller than other 'non-pole' terms and we do not show it in Fig. 9.

V. RESULTS AND DISCUSSION

A. Database

Here we briefly discuss the reaction data base used in the calculations. To simplify the analysis the S_{11} and P_{11} πN partial waves are directly constrained by the single energy solutions (SES) derived by GWU(SAID) [16].

The experimental data on the $\pi^- p \to \pi^0\pi^0 n$ reaction are taken from [26]. These measurements provide high statistics data on the angular distributions $\mathrm{d}\sigma/d\Omega_{\pi\pi}$ where $\Omega_{\pi\pi}$ is the scattering angle of the $\pi\pi$ pair (or the final nucleon in c.m.). This data are accompanied by the corresponding statistical and systematical errors. No such information is available for the mass distributions in [26]. These observables are provided in a form of weighted events without systematic and statistical uncertainties. To use them in the data analysis we rescale them with the requirement that the integrated distributions should reproduce the total cross section of the $\pi^- p \to 2\pi^0 n$ reaction. We also assign about 10% error bars to each mass bin to perform the χ^2 minimization. Starting from 1.46 GeV the excitation of $N^*(1520)$ starts to be important. Already at this energy a small contribution from the spin $J = \frac{3}{2}$ partial wave could modify the angular and mass distributions. Because of this reason we do not try to fit the data above 1.46 GeV.

B. Elastic πN scattering

The resonance couplings are constrained by simultaneous descriptions of the S_{11} and P_{11} πN single energy solutions from GWU(SAID) and the data from the Crystal Ball measurements [26]. The results of our calculations are shown in Fig. 10 in comparison with the πN elastic scattering amplitudes from GWU group [16].

The present calculations demonstrate the good description of SES in the whole energy region. The small rise in the S_{11} partial wave amplitude is due to the tail of the $N^*(1535)$ resonance. The t-channel ρ- and σ-meson exchanges are found to be important for the description of the real part of the S_{11} amplitude at low energies.

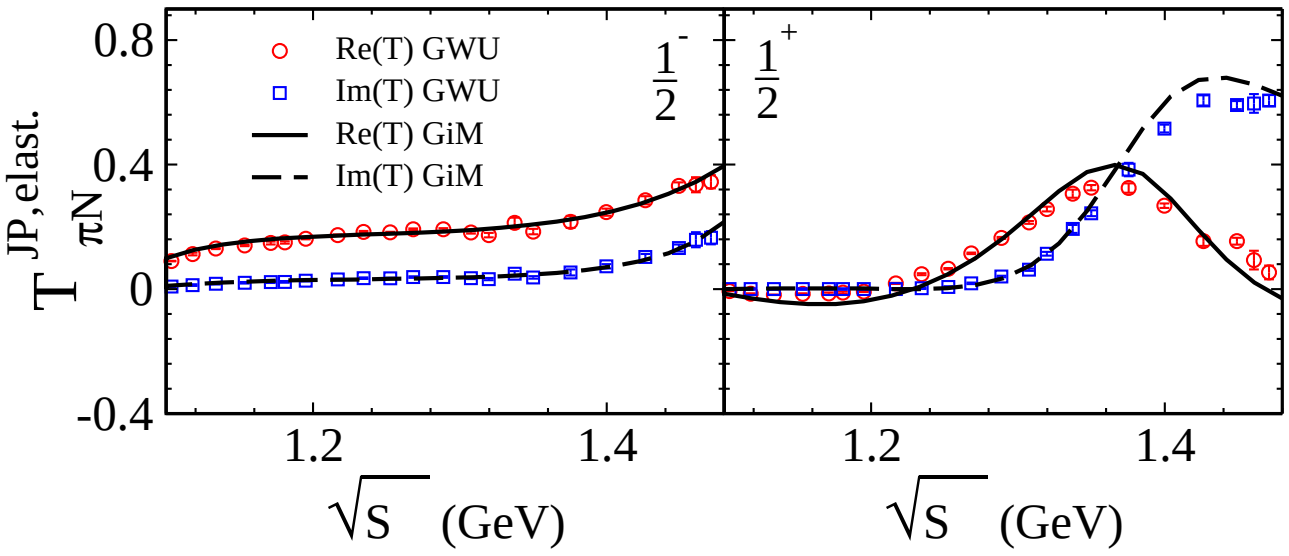

FIG. 10: (Color online) the elastic πN partial wave amplitudes vs. the energy independent solutions from the GWU analysis [16].

C. Reaction $\pi^- p \to \pi^0\pi^0 n$

The calculated differential cross sections are shown in Fig. 11 in comparison with the Crystal Ball data as a function of the c.m. energy. The measurements demonstrate a rapid rise of the cross sections at the energies 1.3-1.46 GeV. Similar to [33, 37] we identify this behavior as an indication for the strong contribution coming from the Roper resonance. Indeed, the resulting πN inelasticities from the GWU(SAID) [16] analysis indicate that the P_{11} partial wave dominates the inelastic transitions at these energies. The inelasticity from the S_{31} channel is about three times less than that from P_{11}. At the same time the $\Delta(1620)$ is strongly coupled to the $2\pi N$ final state through the $\pi\Delta(1232)$ decay [20]. Since the contribution from the σN subchannel is found in the present work to be about twice as large than that of $\pi\Delta(1232)$ is it safe to neglect the possible effect from the $\Delta(1620)$ resonance in the first approximation. We also allow the $N^*(1535)$ resonance decays to the $\pi\Delta(1232)$ and σN isobar final states which are however found to be negligible. At energies close to 1.5 GeV the obtained cross section slightly overestimates the experimental data at backward and underestimates them at forward scattering angles. This is a region where the $N^*(1520)$ starts to play a dominant role. We conclude that the contribution from the D_{13}

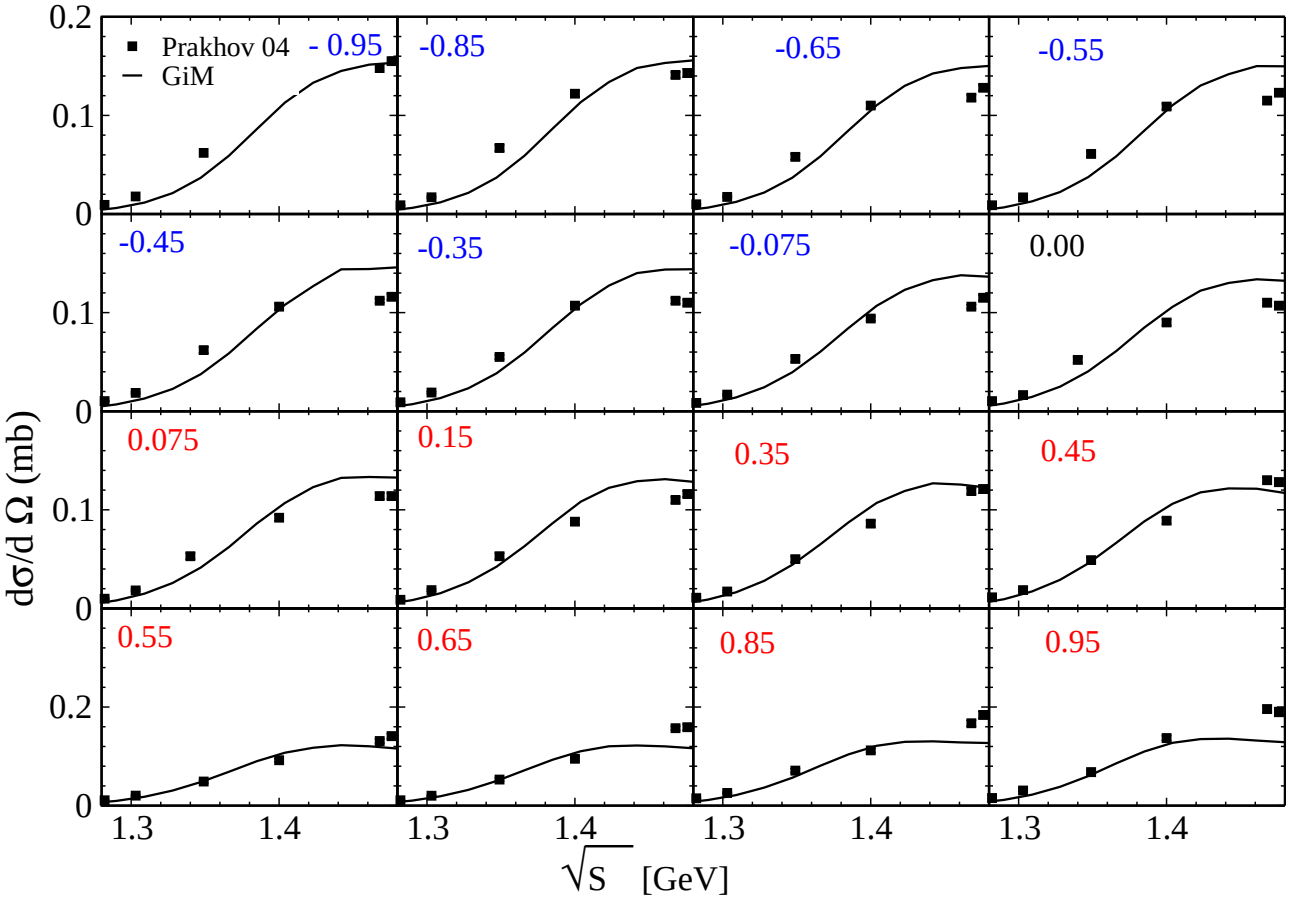

FIG. 11: (Color online) reaction $\pi^- p \to \pi^0\pi^0 n$: differential cross section as a function of the c.m. energy at fixed scattering angles vs the experimental data from [26]. The numbers in the upper left corner give $\cos\theta_N$.

partial wave should be included for the successful description of the data at 1.5 GeV. The effect from the missing spin $J = \frac{3}{2}$ amplitude is also seen in the angular distributions at the energy 1.476 GeV presented in Fig. 12. The experimental data demonstrate the increase at forward and backward angles which is not fully reproduced by the present calculations. We conclude that the missing contributions from the $N^*(1520)$ resonance could be responsible for the effect. The impact of this resonance on the data analysis is estimated in Section V E.

At lower energies the angular distributions show a moderate dependence on the nucleon scattering angle. As discussed in Section IV the separation of the σN and $\pi\Delta(1232)$ isobar channels from this observable turns out to be difficult. The difference between the production

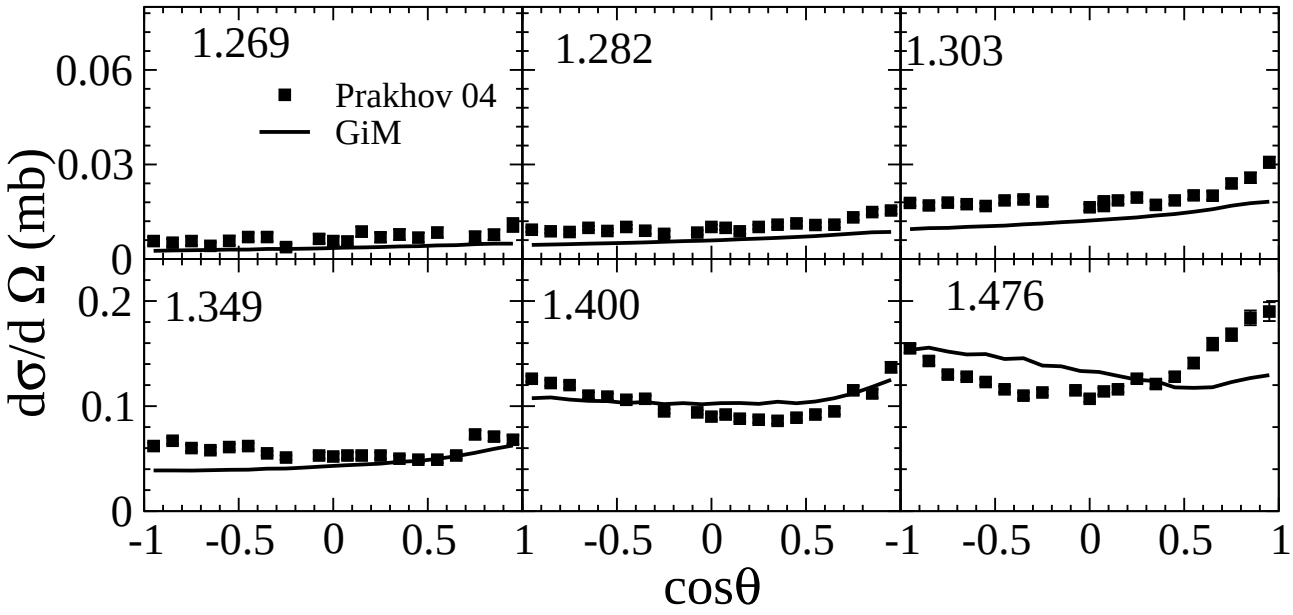

FIG. 12: Reaction $\pi^- p \to \pi^0\pi^0 n$: differential cross section as a function of the c.m. energy at fixed scattering angles vs the experimental data from [26]. The numbers in the upper left corner give the c.m. energy $\sqrt{s}$.

mechanism is expected to be more pronounced in the invariant mass distributions. They are shown in Fig. 13. Close to threshold the Crystal Ball data demonstrate a shift to the higher invariant masses for all energies up to 1.5 GeV whereas the three-body phase space tends to have a maximum at lower $m^2_{\pi^0\pi^0}$. Since the imaginary part of the πN P_{11} elastic amplitude at the energy $\sqrt{s}$ =1.303 GeV, see the right panel of Fig. 10 , is small the effect from the Roper resonance is also expected to be small. As discussed in Section IV the effect from the nucleon Born term in the $\pi\Delta(1232)$ channel is less significant close to threshold. In the present calculations the main contributions to the $\pi^- p \to \pi^0\pi^0 n$ reaction close to threshold are driven by t-channel pion exchange. This mechanism produces the invariant distributions which are shifted to the higher $\pi^0\pi^0$ invariant masses. However, the present calculations do not completely follow the experimental data at 1.303 and 1.349 GeV. It is interesting that the calculations of [37] also underestimate the mass distributions at the same energy though using a different ansatz for the non-resonant part of the production amplitude. The missing contributions are also seen in the angular cross sections at the same energies shown in Fig. 12. However in the latter case the effect is less pronounced since it is smeared out over a large kinematic region. It is not clear whether the missing strength is

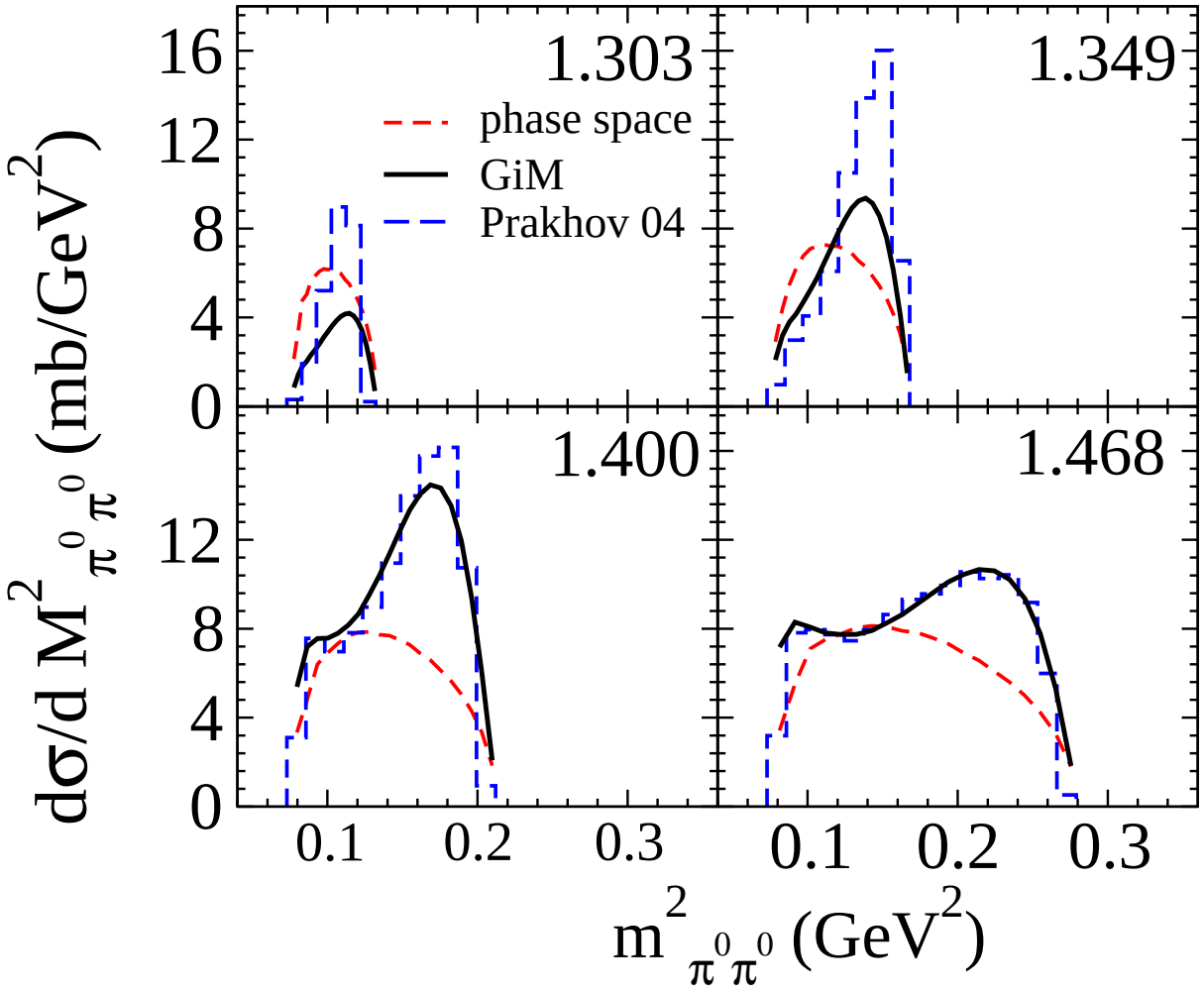

FIG. 13: (Color online) reaction $\pi^- p \to \pi^0\pi^0 n$: differential cross section as a function of $m^2_{\pi\pi}$ at fixed c.m. energies vs the experimental data from [26] (dashed).

associated with the neglected S_{31}-partial wave contributions or whether it could be related to the underestimation of the $\pi\pi$ correlations in the isoscalar channels. We postpone this problem to a future study.

In the region of the Roper resonance our calculations are able to describe the mass distributions rather satisfactorily. Also in this region the production strength is shifted to higher invariant masses $m^2_{\pi^0\pi^0}$. At the same time a peak at small $m^2_{\pi^0\pi^0}$ becomes also visible. In [26] the authors identify this behavior with a strong decay of the $N^*(1440)$ state into the final $\pi\Delta(1232)$ subsystem. At the same time a large decay branching ratio into the latter final state would lead to the more pronounced two-peak structure as demonstrated in Fig. 8. In the present calculations the fit tends to decrease the magnitude of the $\pi\Delta(1232)$

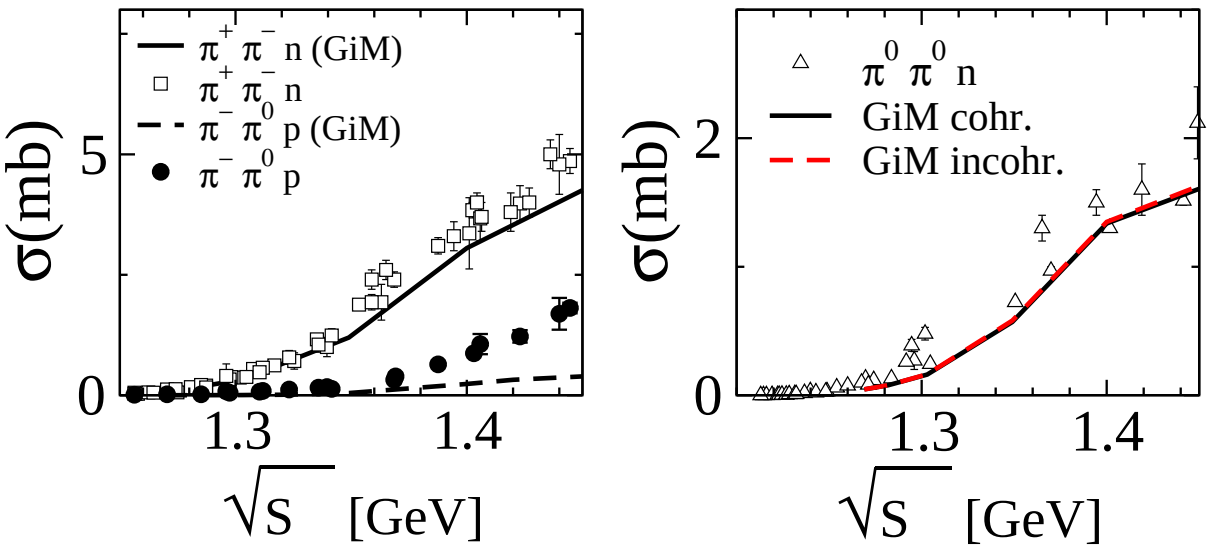

FIG. 14: (Color online) total cross section $\pi^- p \to \pi^+\pi^- n$, $\pi^-\pi^0 p$ (left) and $\pi^- p \to \pi^0\pi^0 n$(right) vs experimental data [52].

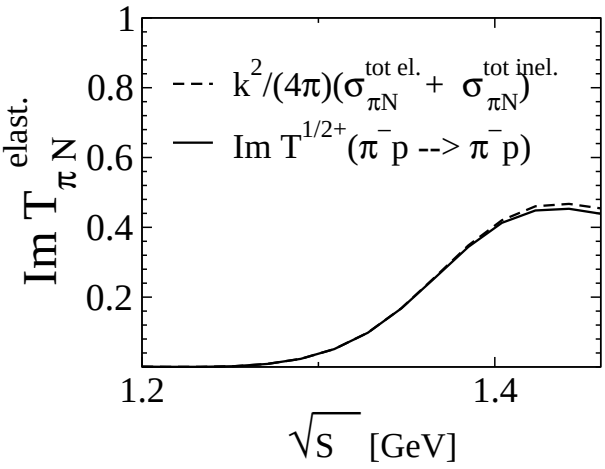

FIG. 15: The left (solid line) and right part (dashed line) of the optical theorem Eq.(4).

production and compensate it by enhancing the strength into σN. The obtained decay branching ratio of $N^*(1440)$ for the σN channel is about twice as large as for the $\pi\Delta(1232)$.

Both the small peak at small and the broad structure at large invariant masses are well reproduced indicating an important interplay between the σN and $\pi\Delta(1232)$ production mechanism. It is interesting that the isoscalar correlations in the $\pi\pi$ rescattering are also

found to be necessary [37] in order to reproduce the asymmetric shape of the mass distributions. Hence the result of the present study and those from [37] are opposite to the conclusion drawn in [26] where no effect from the σN production is found. Though the $\pi\Delta(1232)$ production produces a two-peak structure only the first one at small $m^2_{\pi^0\pi^0}$ is visible at energies 1.4-1.468 GeV. Within the present calculation the second peak at high $m^2_{\pi^0\pi^0}$ is not seen because of the large σN contributions. In the present study $\pi^0\pi^0 n$ production is calculated as a coherent sum of isobar contributions. Though the interference effect are important they are found to be very small at the level of the total cross sections.

The results for the total cross sections are shown in Fig. 14. The present calculations demonstrate a very good description of the experimental data in the region of the Roper resonance.

D. Unitarity

Unitarity is a one of the key issues in the baryon resonance analysis. It relates the imaginary part of the elastic πN scattering to the elastic and inelastic total partial wave cross sections in form of the optical theorem Eqs. (3,4). In this study the three-body unitarity is strictly maintained only up to interference terms between the isobar channels. This raises the question to which extent the interference between the $\pi\Delta(1232)$ and σN channels violates the constraint of Eq. (4). The difference between the coherent and incoherent production is shown on right panel of Fig. 14. The solid(dashed) line corresponds to the case where the total cross section is calculated taking into account (neglecting) the interference between isobar channels. Both curves almost coincide indicating a very small difference between coherent and incoherent production in the present calculations. Note that the interference could still have a visible impact on the e.g. angular distributions. However being integrated over the three-body phase space its effect is found to be small in the total cross sections. This indicates that the contributions from the graphs (e)-(j) in Fig. 3, which are neglected in the present study, are expected to be small.

The left and the right parts of the optical theorem of Eq. (4) for the P_{11} partial wave are shown in Fig. 15. The solid curve corresponds to the imaginary part of the elastic $\pi^- p \to \pi^- p$ scattering . It can be evaluated from the imaginary part of the πN partial wave

amplitude shown in Fig. 10 as follows:

$$\text{Im } T^{\frac{1}{2}^+}_{\pi^- p\to\pi^- p}(\sqrt{s}) = \frac{2}{3}\,\text{Im } T^{\frac{1}{2}^+}_{\pi N}(\sqrt{s}), \tag{22}$$

where $\frac{2}{3}$ stands for an isospin factor.

To check the optical theorem the $\pi^- p \to \pi^-\pi^+ n$ and $\pi^- p \to \pi^-\pi^0 p$ total cross sections have been calculated, see left panel of Fig. 14. Since the isospin $T_1^{\frac{3}{2}}$ contributions which are neglected in the present calculations could be significant in these reactions [10] the description of these channels in terms of only $\pi\Delta$ and σN cannot be fully complete. Therefore, the results in the left panel of Fig. 14 are inelastic flux into these channels exclusively produced by the $\pi\Delta$ and σN (for $\pi^-\pi^+ n$) in the P_{11} wave channel. Note also that only the sum of these two quantities is fixed here due to the optical theorem. The effect from missing contributions is more pronounced in the $\pi^- p \to \pi^-\pi^0 p$ scattering. In fact, in the present calculations this reaction is completely dominated by $\pi\Delta$ which is clearly not enough to account for the total inelasticity in this channel.

The dashed curve in Fig. 15 represents the sum of the total P_{11}-wave cross sections for the elastics $\pi^- p \to \pi^- p$ and all inelastic $\pi^- p \to \pi^0 n$, $\pi^0\pi^0 n$, $\pi^+\pi^- n$, and $\pi^0\pi^- p$ transitions multiplied by the normalization factor $k^2(4\pi)^{-1}$ according to Eq. (4). The contributions to the $2\pi N$ final states are calculated coherently. For the total $\pi N \to 2\pi N$ cross section evaluated incoherently the condition of the optical theorem is fulfilled by construction. For this quantity the right part of Eq. (4) practically coincides with the left part of Eq. (4) and therefore is not shown here. The effect of the interference between the isobar channels in the total cross sections is found to be small. The comparison of the left and right hand side of the Eq. (4) in Fig. 15 demonstrates that the condition of the optical theorem for the three-body unitarity is fulfilled with good accuracy.

Since unitarity relates both πN elastic and $2\pi N$ reactions one could expect that all $2\pi N$ total cross sections should also be explained once unitarity is fulfilled. We stress here that in the present work we limited our calculations to the $IJ^P{=}\frac{1}{2}\frac{1}{2}^{\pm}$ partial waves. Thus, in these spin-isospin channels the constraints of Eq. (4) are fulfilled for each term up to a very small interference effect as discussed above. Therefore the remaining isospin $T_1^{\frac{3}{2}}$ component contributed by the ρN channel not included here, could be still important for the description of the $\pi^-\pi^0 p$ and $\pi^+\pi^- n$ final states.

E. Resonance parameters

The properties of the nucleons resonances are defined by the corresponding pole positions and residues. However, for unstable particles the residues become dependent on the invariant isobar masses. One of the possible ways to overcome this problem is to define these quantities as an integral over the corresponding isobar spectral function. Due to the complexity of the structure of the isobar amplitudes the poles and residues of the $2\pi N$ amplitude will be discussed elsewhere. Here we provide the Breit-Wigner parameters of the resonances. Also in this case the width of the resonance decay into the isobar final state depends on the invariant mass of the unstable particle. Therefore the quantities of interest are calculated as an integral over the corresponding spectral function, see Appendix E.

The extracted resonance properties are listed in Table II in comparison with the results from other studies. The errors of the extracted resonance parameters have been obtained by combining results from several fits with χ^2 values within 5% deviation from the minimal value. The obtained validity ranges derived with this method are in general larger than those extracted from the correlation matrix.

Since the analysis is done for energies below the ηN production threshold the parameters of $N^*(1535)$ cannot be fully constrained. The mass is found to be in a wide range with the central value larger than in our previous calculations [7]. The decay branching ratio $R_{\pi N}$ into the πN final state is, however, very close to our previous result [7]. We obtain almost zero values for the $R_{\sigma N}^{N(1535)}$ and $R_{\pi\Delta(1232)}^{N(1535)}$. This conclusion is in line with other findings, see Table II.

The mass of the Roper resonance is lower than that found in our previous calculations. We obtain a quite large total decay width of $N^*(1440)$ which is, however, smaller than that extracted in previous work [7]. The decay strength for the πN channel is very close to the values given by PDG and other groups. The obtained branching ratio $R_{\sigma N} = 27\%$ agrees very well with the recent result of the KSU group [28]. However they find an almost twice lower branching ratio for the decay of $N^*(1440)$ into the $\pi\Delta(1232)$ subchannel. At the same time they get a slightly larger value for the $R_{\pi N} = 64.8\%$ which should be compared with $R_{\pi N} = 61\%$ derived here. The remaining decay flux of about 1.5% is associated with the ρN isobar final state [28]. An opposite conclusion is drawn by the BoGa group [19]. They find a larger decay strength for the $\pi\Delta(1232)$ subchannel. The σN decay flux of the

N^*	mass	Γ_{tot}	$R_{\pi N}$	$R_{\sigma N}$	$R_{\pi\Delta(1232)}$	Reference
$N^*(1535)\,\frac{1}{2}^-$	1.544^{+6}_{-23}	127^{+30}_{-9}	36^{+4}_{-3}	0^{+1}	0^{+1}	this work
	1.526^{+2}_{-2}	131^{+12}_{-12}	35^{+3}_{-3}	ng	ng	GiM12 [7]
	1.535^{+10}_{-10}	150^{+25}_{-25}	45^{+10}_{-10}	2^{+1}_{-1}	0^{+1}	PDG12[20]
	1.519^{+5}_{-5}	128^{+14}_{-14}	54^{+5}_{-5}	ng	$2.5^{+1.5}_{-1.5}$	BoGa12[19]
	1.538^{+1}_{-1}	141^{+4}_{-4}	37^{+1}_{-1}	$1.5^{+0.5}_{-0.5}$	$2.5^{+1.5}_{-1.5}$	KSU[28]
$N^*(1440)\,\frac{1}{2}^+$	1.478^{+17}_{-27}	569^{+30}_{-240}	61^{+2}_{-7}	27^{+4}_{-9}	12^{+5}_{-3}	this work
	1.515^{+15}_{-15}	605^{+90}_{-90}	56^{+2}_{-2}	ng	ng	GiM12 [7]
	1.440^{+30}_{-20}	300^{+150}_{-100}	65^{+10}_{-10}	15^{+5}_{-5}	25^{+5}_{-5}	PDG12[20]
	1.430^{+8}_{-8}	365^{+35}_{-35}	62^{+3}_{-3}	17^{+7}_{-7}	21^{+8}_{-8}	BoGa12[19]
	1.412^{+2}_{-2}	248^{+5}_{-5}	$64.8^{+0.9}_{-0.9}$	27^{+1}_{-1}	$6.5^{+0.8}_{-0.8}$	KSU[28]
	1.458^{+12}_{-12}	363^{+39}_{-39}	ng	ng	$40.5^{+17.5}_{-17.5}$	JM [53]

TABLE II: Breit-Wigner resonance parameters obtained in the present study. The decay branching ratios are given in percents. The relevance intervals are shown by the upper (lower) subscripts. 'ng' - not given.

Roper resonance is also found to be large: 17%. This values is somewhat smaller than the $\pi\Delta(1232)$ decay fraction.

Both in the BoGa and the present analysis the extracted parameters have large error bars. Within the validity limits the results of this study are overlapping with the findings of [19]. The result of the JM [53] analysis of the CLAS electroproduction data demonstrates a large $\pi\Delta(1232)$ decay fraction of $N^*(1440)$. The central value of 40% is about 6 times larger than that obtained in KSU calculations [28]. Using the quoted values $R_{\rho N}^{N(1440)} < 2\%$ with the lower bound for $R_{\pi\Delta(1232)}^{N(1440)} = 40.5 - 17.5 = 23\%$ from [53] and taking $R_{\pi N}^{N(1440)} = 61\%$ as dictated by the analysis of the πN inelasticities on gets $R_{\sigma N}^{N(1440)} < 16\%$ as an upper limit for the σN branching ratio of $N^*(1440)$. Since the decay properties of $N^*(1440)$ listed in Table II are obtained using different theoretical frameworks and different reaction database it is not clear whether the difference between various analysis could be adresses to the model assumptions or related to a lack of experimental input. One may hope that the combined analysis of photon and pion incuduced reaction would help to pin down the parameters of

$N^*(1440)$.

One of the largest sources of uncertainties in the present calculations is related to the possible influence of the $N^*(1520)$ state on the $\pi^- p \to \pi^0\pi^0 n$ production. Since the contribution from the $N^*(1520)$ resonance is neglected in the present calculation we translate this effect into errors of the extracted resonance parameters. The contribution from $N^*(1520)$ can be estimated from the comparison of the πN inelasticities in the $J = \frac{1}{2}^+$ and $J = \frac{3}{2}^-$ partial waves. These quantities are evaluated in [54] and shown in Fig. 16. The $J^P = \frac{3}{2}^-$ inelastic cross section rapidly rises starting from 1.42 GeV indicating the importance of the $N^*(1520)$ state at energies above 1.46 GeV. To estimate the influence of the $J = \frac{3}{2}^-$ partial wave on the width of N(1440) we construct an additional data set where the original $\pi^- N \to \pi^0\pi^0 N$ experimental data are scaled with the common scaling factor $f_s(\sqrt{s}) = (\sigma_{\text{inel.}}^{\frac{1}{2}\frac{1}{2}^+} - \sigma_{\text{inel.}}^{\frac{1}{2}\frac{3}{2}^-})/\sigma_{\text{inel.}}^{\frac{1}{2}\frac{1}{2}^+}$. Here $\sigma_{\text{inel.}}^{IJ}$ is a total πN inelastic partial wave cross section for the given isospin I and spin J as shown in Fig. 16. Then the parameters of N(1440) are again extracted by making an additional fit to the scaled data. The deviation from the original parameters indicates the influence of the $\text{J}^P\text{I}=\frac{1}{2}^-\frac{3}{2}$ wave on the Roper resonance parameters. Taking this effect into account we obtain a large error interval for the total width of $N^*(1440)$. This is a very conservative estimate of the effect of the $N^*(1520)$ state. We stress that in the case of the large ρN decay fraction of $N^*(1520)$ [20] its actual impact on the $\pi^0\pi^0 n$ production could be smaller than concluded from the simple comparison of the πN inelasticities. The contributions from isospin $I = \frac{3}{2}$ partial waves are found to be small, see Fig. 16.

F. Partial wave analysis of the $\pi N \to \pi N$, $2\pi N$ reactions

The inelastic partial wave cross sections calculated in this work are shown in Fig. 17 in comparison with the results obtained from the SES extracted in [10]. The energy-dependent solutions from the latter work are also shown in the same figure. Our results demonstrate larger inelastic contributions in the σN channel than those extracted by Manley et. al. On the other hand the agreement in the $\pi\Delta$ subchannel is good. The difference between the GiM results and those from [10] is also visible in Fig. 18 where the total P_{11} πN inelasticities are presented in comparison with the results from the GWU analysis [16]. Above 1.4 GeV the $2\pi N$ cross section from [10] tends to be lower than the P_{11} πN inelasticity extracted in by the GWU group [16]. This could be an indication for the inelastic contributions from the

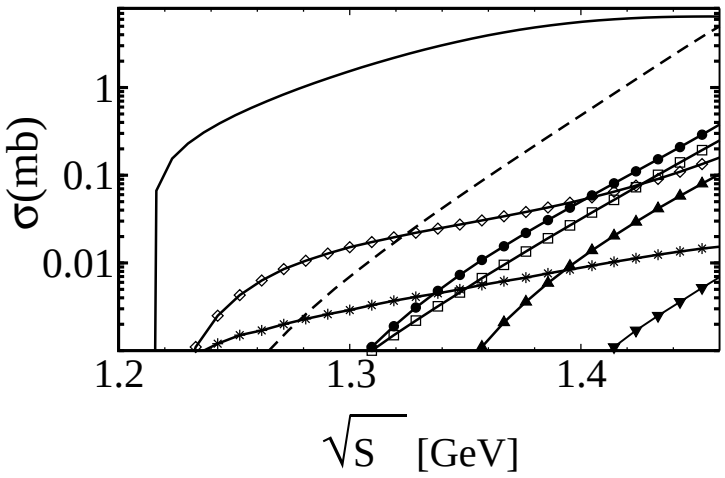

FIG. 16: Comparison of the πN partial wave inelasticities. Notation is as follows: (▲–▲): $J^PI=\frac{1}{2}^-\frac{3}{2}$, (▼–▼): $\frac{3}{2}^+\frac{3}{2}$, (∗–∗): $\frac{1}{2}^+\frac{3}{2}$, (□–□): $\frac{3}{2}\frac{3}{2}^-$, (◇–◇): $\frac{3}{2}\frac{3}{2}^+$, (•–•): $\frac{1}{2}\frac{1}{2}^-$, (——): $\frac{1}{2}\frac{1}{2}^+$, (– –): $\frac{1}{2}\frac{3}{2}^-$.

e.g. $3\pi N$ channel. The difference between the πN inelasticity and the $2\pi N$ reaction cross section could amount up to 1.5mb at $\sqrt{s} = 1.46$GeV. In the present study the possible effect from the $3\pi N$ production has been neglected and the whole inelastic flux moves into the σN channel. Thus we obtain a larger σN contributions above 1.4 GeV as in the analysis of [10], see the left panel of Fig.17. Obviously conclusions on effects from the $3\pi N$ channel can only be drawn when this final state is explicitly included in calculations preserving the unitarity constraint.

The P_{11} πN inelasticity calculated from GiM amplitudes is generally lower than that obtained from the GWU analysis. The reason is that the real and imaginary parts of the elastic πN amplitudes tend to be slightly larger than the P_{11} GWU solution, see Fig.18. Due to unitarity this leads to somewhat lower inelastic reaction cross section than obtained in [16]. Note that in the present study the combined analysis of $\pi N \to \pi N$, $2\pi N$ transitions is made assuming only S_{11} and P_{11} partial wave contributions. The inclusion of higher partial waves and additional decay channels (e.g. ρN) could lead to the re-distribution of the inelastic flux between the various partial wave amplitudes of the $2\pi N$ production. Thus further extensions of the model are required for a more accurate extraction of the partial wave contributions.

Since the σN and $\pi\Delta$ partial wave amplitudes obtained in this study have an additional

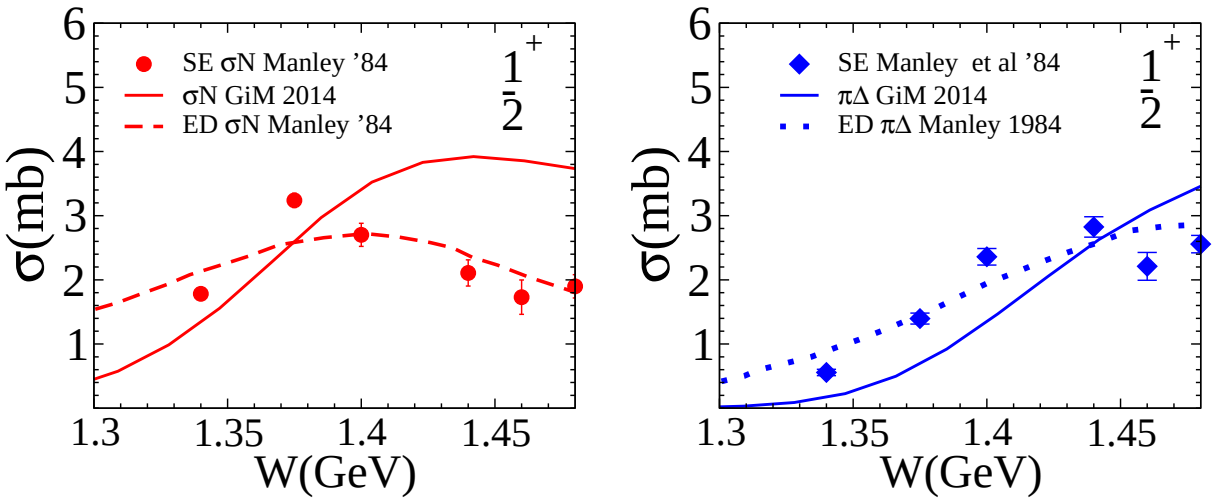

FIG. 17: (Color online) $J^P = \frac{1}{2}^+$ reaction cross sections $\sigma_{\pi N\to\sigma N}$ (left) and $\sigma_{\pi N\to\pi\Delta(1232)}$ (right) in comparison with the single energy(SE) and energy-dependent (ED) results from Manley'84[10].

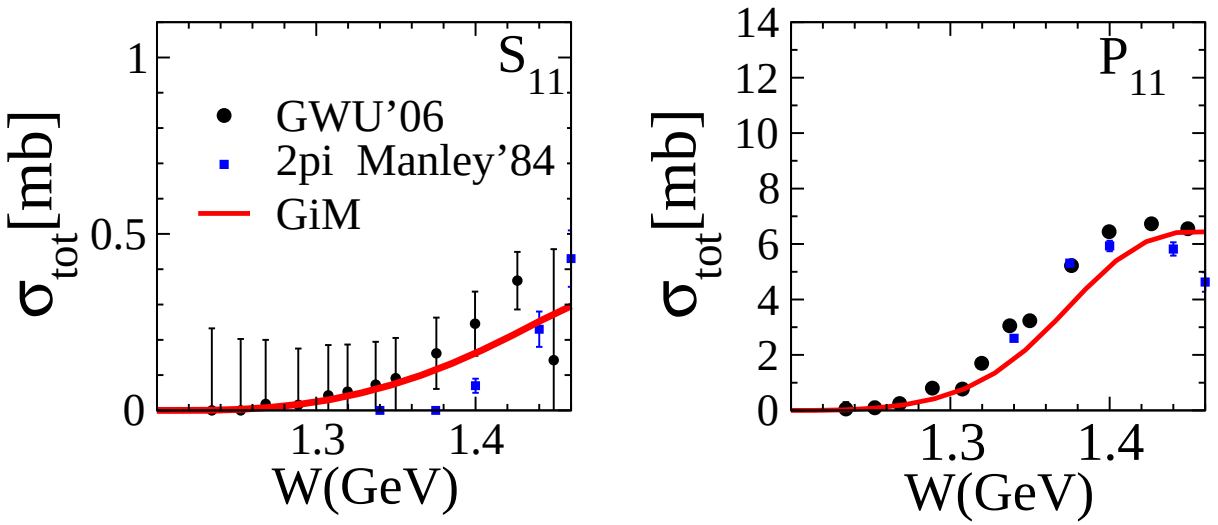

FIG. 18: (Color online) the S_{11} (left) and P_{11} (right) πN inelasticities vs the results from GWU [16] and the 2π cross section from Manley et al [10].

dependence on the isobar mass the direct comparison of our results with the SES from [10] is difficult. The reason is that the dependence on the isobar mass is neglected in [10]. These amplitudes are normalized to give the reaction cross section in the form

$$\sigma_i^{JP}(\sqrt{s}) = \frac{4\pi}{k^2}(J+\frac{1}{2})|T_i^{JP}(\sqrt{s})|^2, \tag{23}$$

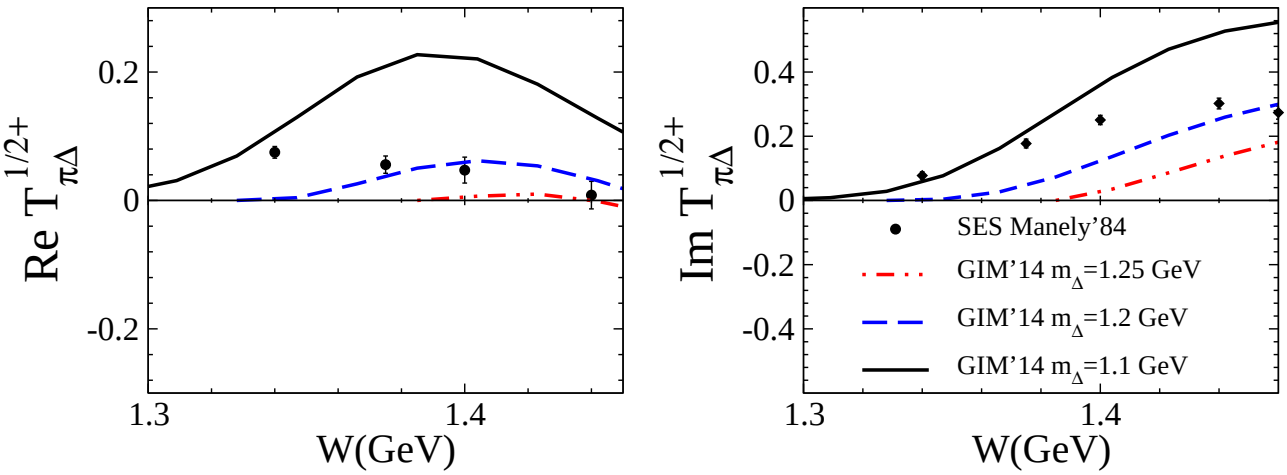

FIG. 19: (Color online) $J^P = \frac{1}{2}^+$ $\pi N \to \pi\Delta(1232)$ amplitude: the real(left) and imaginary (left) parts of the isobar production amplitudes for different values of the isobar-mass. The GiM amplitudes are normalized according Eq. (27). The SES from Manley et al [10] are presented by filled circles.

with $i = \pi\Delta(1232), \sigma N$. The same quantity in the GiM calculations is given in terms of the integral over the isobar mass μ_i :

$$\sigma_i^{JP}(\sqrt{s}) = \frac{4\pi}{k^2}(J+\frac{1}{2})\int_{\mu^2_{\rm min}}^{\mu^2_{\rm max}} |T_i^{JP,\,\rm GiM}(\sqrt{s},\mu^2_{\gamma_i})|^2 A_{\gamma_i}(\mu^2_{\gamma_i})d\mu^2_{\gamma_i}, \tag{24}$$

where $A_{\gamma_i}(\mu^2)$ is a spectral function of the isobar $\gamma_i = \sigma, \Delta(1232)$. If $T_i^{JP,\,\rm GiM}(\sqrt{s},\mu^2)$ had no μ^2-dependence the Eq. (24) would reduce to the form which is similar to Eq. (23)

$$\sigma_i^{JP}(\sqrt{s}) = \frac{4\pi}{k^2}(J+\frac{1}{2})|T_i^{JP,\,\rm GiM}(\sqrt{s})N_i(\sqrt{s})|^2, \tag{25}$$

up to the additional normalization factor

$$N_i(\sqrt{s}) = \sqrt{\int_{\mu^2_{\rm min}}^{\mu^2_{\rm max}} A_{\gamma_i}(\mu^2_\gamma)d\mu^2_{\gamma_i}}. \tag{26}$$

This factor takes into account the propagation and decay of an isobar. In Eq. (23) it is absorbed into the normalization of the reaction amplitudes.

To compare our results with those of Manley et al. [10] we therefore multiply our isobar amplitudes by the factor $N_i(\sqrt{s})$:

$$T_i^{JP,\,\rm GiM}(\sqrt{s},\mu_i^2) \to T_i^{JP,\,\rm GiM}(\sqrt{s},\mu_i^2)N_i(\sqrt{s}) \tag{27}$$

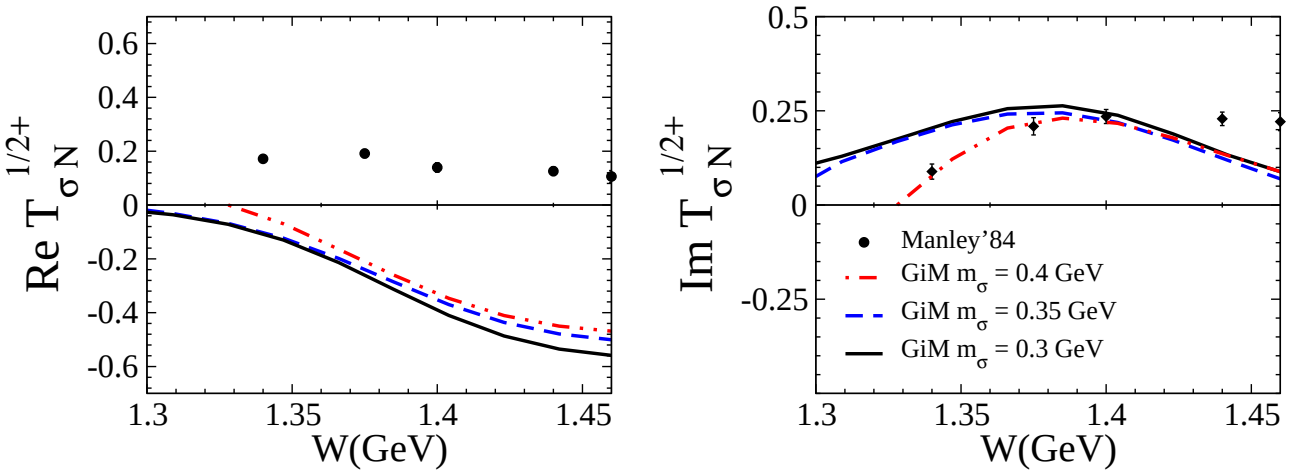

FIG. 20: (Color online) $J^P = \frac{1}{2}^+$ $\pi N \to \sigma N$ amplitude; notation is same as in Fig. 19.

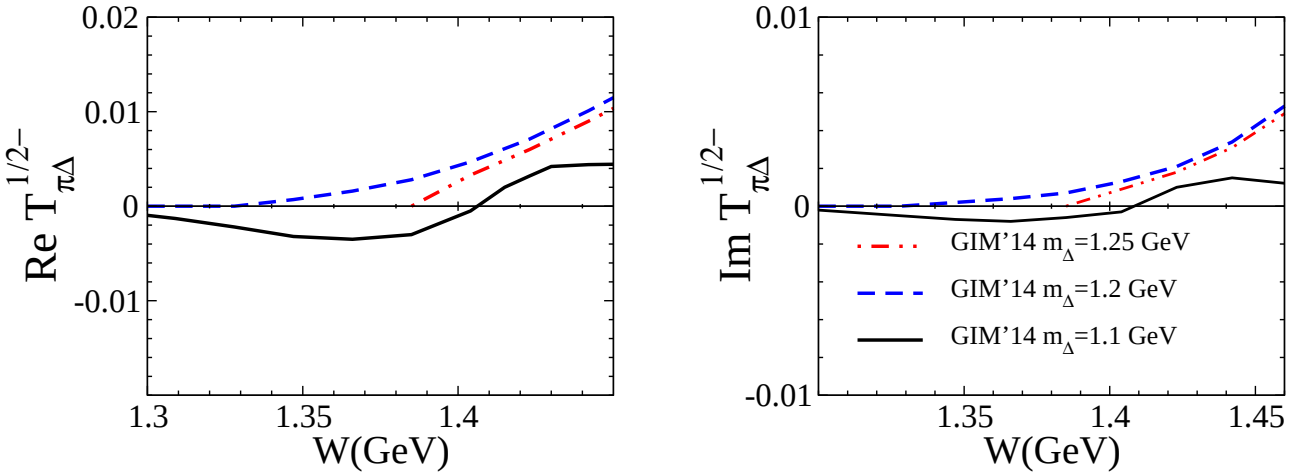

FIG. 21: (Color online) $J^P = \frac{1}{2}^-$ $\pi N \to \pi\Delta(1232)N$ amplitude; notation is same as in Fig. 19.

In Fig. 19 and Fig. 20 the $J^P = \frac{1}{2}^+$ reaction amplitudes as defined in Eq. (27) are presented in comparison with the SES from [10]. Except for the real part of the σN amplitude we find a good agreement with the results from [10]. The major difference is the sign of the $\mathrm{Re}T^{\frac{1}{2}^+}_{\sigma N}$ amplitude. While $\mathrm{Re}T^{\frac{1}{2}^+}_{\sigma N}$ extracted in [10] is positive in the energy region at hand the real part of the GiM-amplitude for the $\pi N \to \sigma N$ transition is negative. The reason for this difference is unclear. The absolute magnitude of $\mathrm{Re}T^{\frac{1}{2}^+}_{\sigma N}$ also tends to be larger than that of [10]. This effect can be attributed to the additional $J^P = \frac{1}{2}^+$ inelastic flux found in [10] as discussed above. The inclusion of the $3\pi N$ channel would bring an additional constraint to check the contribution from this channel.

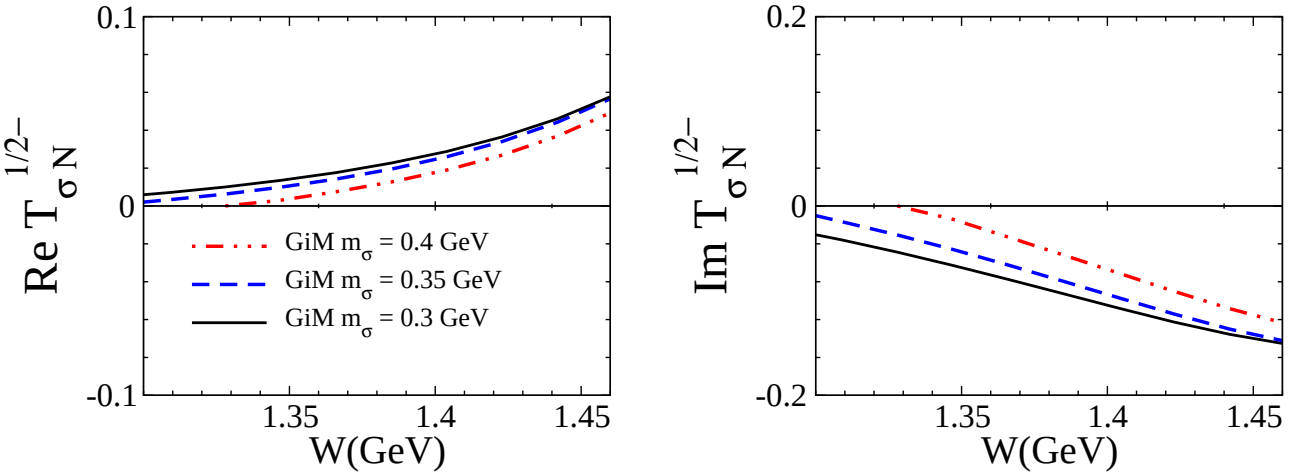

FIG. 22: (Color online) $J^P = \frac{1}{2}^-$ $\pi N \to \sigma N$ amplitude; notation is same as in Fig. 19.

Our calculations demonstrate that the dependence on the isobar masses cannot be neglected. Though the σN amplitude factorized in the form Eq. (27) is a smooth function of μ_σ^2 above 1.38 GeV the dependence on the isobar mass becomes more visible at lower energies. Thus, e.g., the imaginary part of $T^{\frac{1}{2}^+}_{\sigma N}$ vanishes for $\sqrt{s} < m_N + \mu_\sigma$. The mass dependence of $T^{\frac{1}{2}^+}_{\pi\Delta}$ shown in Fig.19 is more drastic: both imaginary and real parts of the reactions amplitudes exhibit fast variations as functions of $\mu_{\Delta(1232)}$. Except for the sign at the Re$T^{\frac{1}{2}^+}_{\sigma N}$ amplitudes our calculation demonstrate in general good agreement with the SES from [10]. This agreement is quite remarkable taking into account the difference in theoretical ansatz and in the reaction database used in the analysis.

The isobar amplitudes in the $J^P = \frac{1}{2}^-$ partial wave are presented in Fig. 21 and Fig. 22. The SES solutions from [10] are not available at these energies. In the present study we obtain almost vanishing σN and $\pi\Delta(1232)$ decay branching ratio of the $N^*(1535)$ resonance. As a result the magnitude of the real and imaginary parts of the $J^P = \frac{1}{2}^-$ $\pi\Delta(1232)$ reaction amplitude are very small. The corresponding values for the $\frac{1}{2}^-$-wave for the $\pi N \to \sigma N$ reaction are found to be larger, see Fig. 22. The dominant contribution to this amplitudes comes from the non-resonant t-channel pion exchange. However the overall effect from the $J^P = \frac{1}{2}^-$ reaction amplitudes in the $2\pi N$ production is very small. This is also consistent with the S_{11} πN inelasticity shown in the left panel of Fig. 18 which is about an order of magnitude smaller than that of the $J^P = \frac{1}{2}^+$ scattering.

VI. CONCLUSION

We develop a coupled-channel Lagrangian approach for the partial wave analysis of the $\pi N \to \pi N$, $\pi\pi N$ reactions. The $\pi\pi N$ production is treated in the isobar approximation. In this framework the optical theorem for the three-body unitarity is strictly fulfilled up to interference between the isobar channels. The Bethe-Salpeter equation is solved to obtain the reaction amplitudes. Assuming dominant contributions from the S_{11} and P_{11} partial waves in the σN and $\pi\Delta$ production channels we have performed a partial wave analysis of the $\pi N \to \pi N$ and $\pi^- p \to \pi^0\pi^0 n$ reactions especially well suited to study the properties of the Roper resonance. The calculations demonstrate a good description of both reactions. We conclude that the invariant $\pi^0\pi^0$ mass distributions play a crucial role in the separation of the isobar contributions. The $\pi^- p \to \pi^0\pi^0 n$ reaction close to threshold is dominated by the σN production due to the $t-$channel pion exchange. The nucleon Born term contribution to the $\pi\Delta(1232)$ channel is found to be less significant. Similar effects are also found in the independent study of [47].

For the decay branching ratios of $N^*(1440)$ we obtain $R_{\sigma N}^{N(1440)} = 27^{+4}_{-9}\%$ and $R_{\pi\Delta(1232)}^{N(1440)} = 12^{+5}_{-3}\%$. Our value for $R_{\sigma N}^{N(1440)}$ coincides with the result of Shrestha and Manley [28]. On other hand the central value of $R_{\pi\Delta(1232)}^{N(1440)} = 12^{+5}_{-3}\%$ is almost twice larger than those derived by these authors: $R_{\pi\Delta(1232)}^{N(1440)} = 6.5^{+0.8}_{-0.8}\%$[28].

The comparison of our results with the parameters extracted by the BoGa group $R_{\sigma N}^{N(1440)} = 17^{+7}_{-7}\%$ and $R_{\pi\Delta(1232)}^{N(1440)} = 21^{+8}_{-8}\%$ demonstrates that despite on the visible difference in the central values these quantities could still coincide within their error bars. The extended analysis of the $\pi\pi N$ which includes higher partial waves would help to reduce the uncertainties of the extracted resonance properties.

The present calculations demonstrate a good agreement with the S_{11} and P_{11} πN inelasticites from the GWU analysis. We extract the $\frac{1}{2}^-$- and $\frac{1}{2}^+$-partial wave amplitudes of the σN and $\pi\Delta(1232)$ production. The obtained partial waves have an additional dependence on the isobar masses. The extracted amplitudes are also in good agreement with the results of Manley et al [10], except for the sign of the real part of the σN amplitude.

In the present work the Roper resonance is described as a genuine pole in contrast to the dynamical pole generated by the correlations in the σN subchannel as reported in [36]. Both calculations demonstrate a very good description of the P_{11} πN elastic scattering

amplitudes. This rises a question how these scenarios could be identified in experiment. The study of the $\pi\pi N$ reaction provides a chance to explore these possibilities in more details. If the pole associated with the Roper resonance is dynamically generated due to a strong $t-$ channel exchange in the σN channel one could also expect a substantial contribution from this mechanism to the higher partial waves of the $\pi N \to \pi\pi N$ production. This effect could be more pronounced with increasing scattering energy. At the same time the genuine pole produces in general only minor 'background contributions' due to u-channel exchange; the major effect is seen in the $J^P = \frac{1}{2}^+$ partial wave. The angular distributions could be also different: the strong t-channel exchange ordinarly gives rise at forward angles which can also be identified in the angular distributions. At the same time the $u-$channel mechanism is more important at backward angles. Therefore, a detailed analysis of the $2\pi N$ reaction could help to disentangle various scenarios.

This program cannot be accomplished without a new generation of the high statistic $\pi N \to \pi\pi N$ scattering data. New measurements at the HADES [55] and JPARC [56] facilities would help to resolve to problem.

Acknowledgement

Work supported in part by DFG, grant Le439/7 and SFB/TR 16.

Appendix A: Three-body unitarity for the σN isobar channel

Here we demonstrate the maintenance of the tree-body unitarity Eq. (3) when the pions are produced via σN subchannel. For the sake of clarity isospin indices are omitted. The scattering equation Eq. (14) for the $(\pi/\sigma)N \to (\pi/\sigma)N$ transitions can be rewritten in the form:

$$T^{JP}_{f\,i}(\sqrt{s}) = K^{JP}_{f\,i}(\sqrt{s}) + \mathrm{i}\, T^{JP}_{f\,\pi N} K^{JP}_{\pi N\,i} + \mathrm{i} \int d\mu^2 A_\sigma(\mu^2) T^{JP}_{f\,\sigma N} K^{JP}_{\sigma N\,i}. \tag{A1}$$

By replacing the integral in Eq. (A1) by summation one gets

$$\int_{4m_\pi^2}^{(\sqrt{s}-m_N)^2} d\mu^2 A_\sigma(\mu^2)\, T^{JP}_{f\,\sigma N}(\sqrt{s},\mu^2)\, K^{JP}_{\sigma N\,i}(\sqrt{s},\mu^2) = \sum_l \Delta\mu_l^2\ A_{\sigma_l}(\mu_l^2)\ T^{JP}_{f\,\sigma_l N}(\sqrt{s},\mu_l^2)\, K^{JP}_{\sigma_l N\,i}(\sqrt{s},\mu_l^2). \tag{A2}$$

By introducing the amplitudes and interaction kernel in the form

$$\begin{aligned}
\tilde{T}_{\pi N,\,\sigma_l N} &= T_{\pi N,\,\sigma_l N}(\sqrt{s},\mu_l^2)\sqrt{\Delta\mu_l^2 A_{\sigma_l}(\Delta\mu_l^2)},\\
\tilde{K}_{\pi N,\,\sigma_l N} &= K_{\pi N,\,\sigma_l N}(\sqrt{s},\mu_l^2)\sqrt{\Delta\mu_l^2 A_{\sigma_l}(\Delta\mu_l^2)},\\
\tilde{T}_{\sigma_j N,\,\sigma_l N} &= \sqrt{\Delta\mu_j^2 A_{\sigma_j}(\mu_j^2)}\; T_{\sigma_j N,\,\sigma_l N}(\sqrt{s},\mu_j^2,\mu_l^2)\; \sqrt{\Delta\mu_l^2 A_{\sigma_l}(\mu_l^2)},\\
\tilde{K}_{\sigma_j N,\,\sigma_l N} &= \sqrt{\Delta\mu_j^2 A_{\sigma_j}(\mu_j^2)}\; K_{\sigma_j N,\,\sigma_l N}(\sqrt{s},\mu_j^2,\mu_l^2)\; \sqrt{\Delta\mu_l^2 A_{\sigma_l}(\mu_l^2)},\\
&\ldots, \qquad\qquad\qquad\

provided that the interaction kernel $[\tilde{K}^{JP}]$ is hermitian. The first term in brackets of the right side of the Eq. (A9) denotes the total πN elastic partial wave cross section and the second one is a sum of all inelastic partial wave cross sections. It can be rewritten as

$$\begin{aligned}
\sum_j \sigma^{JP}_{\pi N\to\sigma_j N} &= \frac{4\pi}{k^2}\sum_j |\tilde{T}^{JP}_{\pi N,\,\sigma_j N}|^2 \\
&= \frac{4\pi}{k^2}\sum_j |T^{JP}_{\pi N,\,\sigma_j N}(\sqrt{s},\mu_j^2)|^2\,\Delta\mu_j^2\,A_\sigma(\mu_j^2) \\
&= \frac{4\pi}{k^2}\int_{4m_\pi^2}^{(\sqrt{s}-m_N)^2} d\mu^2 A_\sigma(\mu^2)|T^{JP}_{\pi N,\,\sigma_j N}(\sqrt{s},\mu_j^2)|^2 \\
&= \sigma^{JP}_{\pi N\to\sigma N}, \qquad\qquad (A10)
\end{aligned}$$

where $\sigma^{JP}_{\pi N\to\sigma N}$ is a total σ-meson production cross section for the given total spin J and parity P. It remains to show that $\sigma^{JP}_{\pi N\to\sigma N} = \sigma^{JP}_{\pi N\to\pi\pi N}$ where pions are exclusively produced from the σ-meson decay. The total cross section can be written in the form

$$\begin{aligned}
\sigma^{JP}_{\pi N\to\pi\pi N} = \frac{(2\pi)^4}{4\sqrt{(q_\pi\,p_N)^2 - m_N^2 m_\pi^2}}\int \frac{d^3q_1'}{2E_1'(2\pi)^3}\frac{d^3q_2'}{2E_2'(2\pi)^3}\frac{d^3p_N'}{2E_N'(2\pi)^3} \\
\times\,\overline{|T^{JP}_{\pi N\to\pi\pi N}|^2}\,\delta^4(p_N + q_\pi' - q_1' - q_2 - p_N'), \qquad (A11)
\end{aligned}$$

where p_N', q_1', and q_2', are four-momenta of the final nucleon and the pions respectively, p_N and q_π are momenta of the initial nucleon and the pion. The expression Eq.(A11) can be rewritten in the form

$$\sigma^{JP}_{\pi N\to\pi\pi N} = \frac{1}{8\pi\sqrt{(q_\pi\,p_N)^2 - m_N^2 m_\pi^2}}\int d\mu^2\,dF_2(s,m_N^2,s_{\pi\pi})\,dF_2(\mu^2,m_\pi^2,m_\pi^2)\overline{|T^{JP}_{\pi N\to\pi\pi N}|^2}, \qquad (A12)$$

where the two-body phase spaces are given as

$$\begin{aligned}
dF_2(s,m_N^2,\mu^2) &= \frac{d^3k}{2E_k(2\pi)^3}\frac{d^3p_N'}{2E_N'(2\pi)^3}(2\pi)^4\delta^4(p_N + q_\pi - k - p_N'), \\
dF_2(\mu^2,m_\pi^2,m_\pi^2) &= \frac{d^3q_1'}{2E_1'(2\pi)^3}\frac{d^3q_2'}{2E_2'(2\pi)^3}(2\pi)^4\delta^4(k - q_1' - q_2'), \qquad (A13)
\end{aligned}$$

with $\mu^2 = E_k^2 - \mathbf{k}^2 = (q_1' + q_2')^2$. The transition amplitude $T_{\pi N\to\pi\pi N}$ is given by the expression

$$T_{\pi N\to\pi\pi N} = T_{\pi N,\,\sigma N}(p_N', q_\sigma')\,G_\sigma(q_\sigma'^2)\,V_{\sigma\pi\pi}(q_\sigma', q_1', q_2'), \qquad (A14)$$

where $T_{\pi N,\sigma N}(p'_N, q'_\sigma)$ is a amplitude of the isobar production, $G_\sigma(q'^2_\sigma)$ stands for the σ-meson propagator Eq. (7), and $V_{\sigma\pi\pi}(q'_\sigma, q'_1, q'_2)$ denotes $\sigma\pi\pi$ decay vertex.

Since the two-particle phase space is invariant under inhomogeneous Lorentz transformations the integrals over $dF_2(s_{\pi\pi}, m_\pi^2, m_\pi^2)$ and $dF_2(s, m_N^2, s_{\pi\pi})$ can independently be evaluated in separate reference frames. The integration over $dF_2(\mu^2, m_\pi^2, m_\pi^2)$ is evaluated in the σ-meson rest frame:

$$(2\pi)^4 \int F_2(\mu^2, m_\pi^2, m_\pi^2)|V_{\sigma\pi\pi}(q'_\sigma, q'_1, q'_2)|^2 = 2\sqrt{\mu^2}\,\Gamma_{\sigma\to\pi\pi}(\mu^2) = 2\Sigma_\sigma(\mu^2), \tag{A15}$$

where we use relation between the decay width of the σ-meson $\Gamma_{\sigma\to\pi\pi}(\mu^2)$ and the σ-meson self-energy $\Sigma_\sigma(\mu^2)$ calculated in the ladder approximation to DSE, see Section III B. Using the result of Eq. (A15) and definitions Eqs. (7, 12) the intergral Eq. (A12) becomes

$$\sigma^{JP}_{\pi N\to\pi\pi N} = \frac{1}{4\sqrt{(q_\pi\, p_N)^2 - m_N^2 m_\pi^2}} \int d\mu^2\, dF_2(s, m_N^2, \mu^2)|\overline{T_{\pi N\to\sigma N}}|^2 A_\sigma(\mu^2). \tag{A16}$$

Since $\Sigma_\sigma(\mu^2)$ is invariant under inhomogeneous Lorentz transformations one can evaluate Eq. (A16) in the σN c.m. reference frame which gives

$$\sigma^{JP}_{\pi N\to\pi\pi N} = \frac{4\pi}{k^2} \int_{4\pi^2}^{\sqrt{s}-m_N} d\mu^2 |\overline{T^{JP}_{\pi N\to\sigma N}}|^2 A_\sigma(\mu^2) = \sigma^{JP}_{\pi N\to\sigma N} \tag{A17}$$

where only contributions which the total spin J and parity P have been taken into account. Hence Eq. (A9) reads as

$$\mathrm{Im}\, T^{JP}_{\pi N\to\pi N} = \frac{k^2}{4\pi}\left(\sigma^{JP}_{\pi N\to\pi N} + \sigma^{JP}_{\pi N\to\pi\pi N}\right) \tag{A18}$$

from which follows that the condition of the optical theorem Eq. (3) is fulfilled.

Appendix B: Kinematics of the $\pi N \to 2\pi N$ reaction

The differential cross section for the $\pi N \to \pi\pi N$ transition can be written as

$$\sigma^{\mathrm{coh/incohr}}_{\pi N\to\pi\pi N} = \frac{(2\pi)^4}{4\sqrt{(q_\pi\, p_N)^2 - m_N^2 m_\pi^2}} \int \frac{d^3q'_1}{2E'_1(2\pi)^3}\frac{d^3q'_2}{2E'_2(2\pi)^3}\frac{d^3p'_N}{2E'_N(2\pi)^3} \times |\overline{T^{\mathrm{coher/incohr}}_{\pi N\to\pi\pi N}}|^2 \delta^4(p_N + q'_\pi - q'_1 - q_2 - p'_N), \tag{B1}$$

where p'_N, q'_1, and q'_2 are four-momenta of the final nucleon and the pions, p_N and q_π are momenta of the initial nucleon and the pion. The quantities $\overline{|T^{\rm coher/incohr}_{\pi N\to\pi\pi N}|^2}$ are defined as

$$\begin{aligned}
\overline{|T^{\rm coher}_{\pi N\to\pi\pi N}|^2} &= \frac{1}{2}\sum_{s_i s_f}|T^a_{s_i,\,s_f}+T^b_{s_i,\,s_f}+T^c_{s_i,\,s_f}+T^d_{s_i,\,s_f}|^2,\\
\overline{|T^{\rm incoher}_{\pi N\to\pi\pi N}|^2} &= \frac{1}{2}\sum_{s_i s_f}\left(|T^a_{s_i,\,s_f}|^2+|T^b_{s_i,\,s_f}|^2+|T^c_{s_i,\,s_f}|^2+|T^d_{s_i,\,s_f}|^2\right),
\end{aligned} \tag{B2}$$

where s_i and s_f are spin projections (helicities) of the initial and final nucleon respectively and the amplitudes

$$\begin{aligned}
T^a_{s_i,\,s_f} &= T_{s_i,\,s_f}(\sqrt{s},q'_\sigma,p'_N)\,G_\sigma(q'_\sigma)\,V^{\sigma\pi\pi}(q_\sigma,q'_1,q'_2),\\
T^b_{s_i,\,s_f} &= T_{s_i,\,s_f}(\sqrt{s},q'_\sigma,p'_N)\,G_\sigma(q'_\sigma)\,V^{\sigma\pi\pi}(q_\sigma,q'_2,q'_1),\\
T^c_{s_i,\,s_f} &= \sum_{s_{\Delta_2}} T_{s_i,\,s_{\Delta_2}}(\sqrt{s},p'_{\Delta_2},q'_1)\,G_\Delta(p'_{\Delta_2})\,V^{\Delta\pi N}_{s_{\Delta_2},\,s_f}(p'_{\Delta_2},p'_N),\\
T^d_{s_i,\,s_f} &= \sum_{s_{\Delta_1}} T_{s_i,\,s_{\Delta_1}}(\sqrt{s},p'_{\Delta_1},q'_2)\,G_\Delta(p'_{\Delta_1})\,V^{\Delta\pi N}_{s_{\Delta_1},\,s_f}(p'_{\Delta_1},p'_N)
\end{aligned} \tag{B3}$$

correspond to the contributions from the diagrams (a)-(b) depicted in Fig. 4. The notation is as follows: $p'_{\Delta_2}=(p'_N+q'_2)$ and $p'_{\Delta_1}=(p'_N+q'_1)$ are momenta of the intermediate $\Delta(1232)$ isobar and $s_{\Delta_1}(s_{\Delta_2})$ are its spin projections. Quantities $T_{s_i,\,s_f}(\sqrt{s},q'_\sigma,p'_N)$, $T_{s_i,\,s_{\Delta_2}}(\sqrt{s},p'_{\Delta_2},q'_2)$ and $T_{s_i,\,s_{\Delta_1}}(\sqrt{s},p'_{\Delta_1},q'_1)$ stand for σN and $\pi\Delta(1232)$ production amplitudes obtained by solving the scattering equation Eq. (16). The kinematic of the reaction is shown in Fig. 23. The vector $\mathbf{p'_N}$ lies in the xy-plane. All calculations are performed in the c.m. system of the initial πN state. Since Eq. (16) is also solved in the same reference frame no additional boost for the $T_{s_i,\,s_f}(\sqrt{s},q'_\sigma,p'_N)$, $T_{s_i,\,s_{\Delta_2}}(\sqrt{s},p'_{\Delta_2},q'_2)$ and $T_{s_i,\,s_{\Delta_1}}(\sqrt{s},p'_{\Delta_1},q'_1)$ amplitudes is required. The $T_{s_i,\,s_f}(\sqrt{s},q'_\sigma,p'_N)$ amplitude is directly calculated from the σN partial waves as shown in Appendix C. The isobar production amplitudes $T_{s_i,\,s_{\Delta_2}}(\sqrt{s},p'_{\Delta_2},q'_2)$ and $T_{s_i,\,s_{\Delta_1}}(\sqrt{s},p'_{\Delta_1},q'_1)$ are also calculated from the corresponding partial waves, see Appendix C. Since vectors $p'_{\Delta_1}=(p'_N+q'_1)$ and $p'_{\Delta_2}=(p'_N+q'_2)$ do not lie in the xy-plane the obtained amplitudes are rotated around z-axis by the corresponding azimuthal angles $\phi_{p_{\Delta_1}}$ and $\phi_{p_{\Delta_2}}$ respectively [57].

The $\sigma\pi\pi$ decay vertex $V^{\sigma\pi\pi}(q_\sigma,q'_1,q'_2)$ is obtained from the corresponding interaction Lagrangian. Due to the spin of the $\Delta(1232)$-isobar and the final nucleon the evaluation of

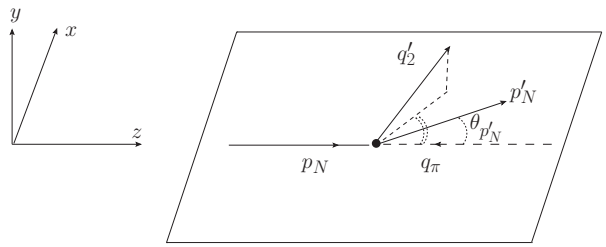

FIG. 23: Kinematics of the reaction $\pi N \to \pi\pi N$

the $\Delta(1232)\pi N$ decay vertices $V^{\Delta(1232)\pi N}_{s_{\Delta_2},s_f}(p'_{\Delta_2},p'_N)$ and $V^{\Delta(1232)\pi N}_{s_{\Delta_1},s_f}(p'_{\Delta_1},p'_N)$ is more involved. The vertices

$$V^{\Delta(1232)\pi N}_{s_{\Delta_j},s_f}(p_{\Delta(1232)_j},p'_N) = \mathrm{i}\frac{f_{\pi N\Delta(1232)}}{m_\pi} I_{\pi N\Delta}[\bar{u}(s_f,p'_N)u^\mu(s_{\Delta_j},p_{\Delta_j})](p_{\Delta_j}-p'_N)_\mu, \qquad \text{(B4)}$$

are derived from the corresponding $\pi N\Delta(1232)$ Lagrangian and evaluated in the c.m. of the initial πN state. In this reference frame $\Delta(1232)$-isobar is moving along the direction defined by a vector sum of the final nucleon $\mathbf{p'_N}$ and the momentum of the pion emitted by $\Delta(1232)$. Using Eqs. (C1) the isobar spin-vectors are first defined in the helicity basis. Then the decay vertex is numerically evaluated for each helicity combination.

Here $I_{\pi N\Delta}$ is an isospin factor, and the spin-vector $u^\mu(s_{\Delta_j},p_{\Delta_j})$ satisfies the Rarita-Schwinger conditions, see Appendix C.

The four-fold differential cross section reads

$$\frac{\mathrm{d}\sigma^{\text{coher/incohr}}}{\mathrm{d}E'_N \mathrm{d}\cos\theta_{N'}\mathrm{d}\Omega_{q'_2}} = \frac{1}{16(2\pi)^5\sqrt{(p_N q_\pi)^2 - m_\pi^2 m_N^2}} \overline{|T^{\text{coher/incohr}}_{\pi N\to\pi\pi N}|^2} \frac{{q'_2}^2 p'_N}{|A\,q'_2 + C\,E'_2|}, \qquad \text{(B5)}$$

where $q'_2 = |\mathbf{q'_2}|$ and $p'_N = |\mathbf{p'_N}|$, $A = 2(\sqrt{s} - E'_N)$, $C = 2p'_N\cos\theta_{\widehat{p'_N,q'_2}}$. $\theta_{\widehat{p'_N,q'_2}}$ is the angle between the vectors $\mathbf{q'_2}$ and $\mathbf{p'_N}$. Defining quantities

$$\begin{aligned}
\alpha &= C^2 - A^2, \\
\beta &= 2C\,(s + m_N^2 - 2\sqrt{s}\,E'_N), \\
\zeta &= B^2 - A^2 m_\pi^2, \\
\mathcal{D} &= \beta^2 - 4\alpha\,\zeta,
\end{aligned} \qquad \text{(B6)}$$

one obtains the expression for q'_2

$$q'_2 = \frac{\beta \pm \sqrt{\mathcal{D}}}{2\alpha}, \qquad \text{(B7)}$$

provided that $\mathcal{D} \geq 0$ and $q'_2 > 0$.

From the Eq. (B5) one can define angular and mass distributions:

$$\begin{aligned}
\frac{\mathrm{d}\sigma^{\mathrm{coher/incohr}}}{\mathrm{d}\Omega_{N'}} &= \frac{1}{16(2\pi)^5\sqrt{(p_N q_\pi)^2 - m_\pi^2 m_N^2}} \int \mathrm{d}E'_N \mathrm{d}\Omega_{q'_2} |\overline{T^{\mathrm{coher/incohr}}_{\pi N\to\pi\pi N}}|^2 \frac{{q'_2}^2 p'_N}{|A\, q'_2 + C\, E'_2|}, \\
\frac{\mathrm{d}\sigma^{\mathrm{coher/incohr}}}{\mathrm{d}m^2_{\pi\pi}} &= \frac{1}{32\sqrt{s}\,(2\pi)^5\sqrt{(p_N q_\pi)^2 - m_\pi^2 m_N^2}} \int \mathrm{d}\Omega_{q'_2} \mathrm{d}\Omega_{N'} |\overline{T^{\mathrm{coher/incohr}}_{\pi N\to\pi\pi N}}|^2 \frac{{q'_2}^2 p'_N}{|A\, q'_2 + C\, E'_2|},
\end{aligned} \tag{B8}$$

where $m^2_{\pi\pi} = s - 2\sqrt{s}\, E'_N + m^2_N$.

Appendix C: Partial wave decomposition of isobar amplitudes

The general details of the partial wave decomposition can be found in [57]. For the $\pi N \to \pi N$, σN transitions we use the expressions which are elaborated in [3]. Here we only consider complications related with the $\pi\Delta(1232)$ channel. The spin-vectors u^μ in the Rarita-Schwinger formalism satisfies the set of constraints

$$\begin{aligned}
(\not{p}_\Delta - m_\Delta) u^\mu(\lambda_\Delta, p_\Delta) &= 0, \\
\gamma_\mu u^\mu(\lambda_\Delta, p_\Delta) &= 0, \\
\partial_\mu u^\mu(\lambda_\Delta, p_\Delta) &= 0.
\end{aligned} \tag{C1}$$

The spin structure of the $(\pi/\sigma) \to \pi\Delta(1232)$ and $\pi\Delta(1232) \to \pi\Delta(1232)$ transitions can be expressed through as

$$\bar{u}^\mu(\lambda'_\Delta, p'_\Delta) A^\mu(p'_\Delta, q'_{\pi/\sigma}; p_N) u(\lambda_N, p_N) \tag{C2}$$

and

$$\bar{u}^\mu(\lambda'_\Delta, p'_\Delta) A_{\mu\,\nu}(p'_\Delta, q'_{\pi/\sigma}; p_\Delta) u^\nu(\lambda_\Delta, p_\Delta) \tag{C3}$$

respectively. In the c.m. of colliding particles the amplitudes of the isobar production are functions of the c.m energy $\sqrt{s}$, isobar mass μ, scattering angle θ and particle helicities : $T_{\lambda,\,\lambda'}(\sqrt{s}, p'_{\Delta_1}, q'_2) = T_{\lambda',\lambda}(\sqrt{s}; \mu, \cos\theta)$

$$T_{\lambda',\lambda}(\sqrt{s}; \mu, \cos\theta) = \mathcal{N}^{-1} \sum_J \frac{2J+1}{4\pi} T^J_{\lambda',\lambda}(\sqrt{s}; \mu) d^J_{\lambda,\lambda'}(\cos\theta), \tag{C4}$$

where $d^J_{\lambda,\lambda'}(\cos\theta)$ is a Wigner d-function, $\lambda'(\lambda)$ is a sum of particle helicities in the final (initial) state, and $\mathcal{N} = -\sqrt{k,k'}/((4\pi)^2 2\sqrt{s})$ is an overall kinematical normalization factor with $k\,(k')$ being initial (final) c.m. momentum. The d-functions is are normalized in the conventional way:

$$\int_{-1}^{+1} \mathrm{d}\cos\theta\ d^J_{\lambda,\lambda'}(\cos\theta)\ d^{J'}_{\lambda,\lambda'}(\cos\theta) = \frac{2}{2J+1}\delta_{J\,J'} \tag{C5}$$

The same formulae of Eq. (C4) is used for the decomposition of the interaction kernel $K_{\lambda',\lambda}(\sqrt{s};\mu,\cos\theta)$.

The inverse transformation is

$$\begin{aligned} T^J_{\lambda',\lambda}(\sqrt{s};\mu) &= (2\pi)\,\mathcal{N}\int_{-1}^{+1}\mathrm{d}\cos\theta\ T_{\lambda',\lambda}(\sqrt{s};\mu,\cos\theta)\ d^J_{\lambda,\lambda'}(\cos\theta), \\ K^J_{\lambda',\lambda}(\sqrt{s};\mu) &= (2\pi)\,\mathcal{N}\int_{-1}^{+1}\mathrm{d}\cos\theta\ K_{\lambda',\lambda}(\sqrt{s};\mu,\cos\theta)\ d^J_{\lambda,\lambda'}(\cos\theta). \end{aligned} \tag{C6}$$

There are four (eight) independent amplitudes to describe the various helicity combinations of $\pi N \to \pi\Delta(1232)$ ($\pi\Delta(1232) \to \pi\Delta(1232)$) transitions. Due to the parity conservation in the strong interaction one can define amplitude with well defined parity $P = \pm 1$ as linear combinations:

$$T^{J\pm}_{\lambda',\lambda}(\sqrt{s};\mu) = T^J_{\lambda',\lambda}(\sqrt{s};\mu) \pm \eta\, T^J_{\lambda',-\lambda}(\sqrt{s};\mu) \tag{C7}$$

where $\eta = \eta_m\eta_B(-1)^{J-s_1-s_2}$ and $s_1(s_2)$ and $\eta_{\mathrm{m}}(\eta_{\mathrm{B}})$ are the spin and the parity of the meson and baryon in the entrance channel.

Appendix D: Isospin decomposition of the $\pi N \to \pi\pi N$ reaction

Due to the isospin conservation all $\pi N \to \pi\pi N$ transitions can be expressed in term amplitudes with well defined isospin. The 'minimal' isospin decomposition would correspond to the separation of the isospin $\frac{3}{2}$ and $\frac{1}{2}$ states. Within the isobar approximation this is already enough to separate contributions between N^* and Δ^* resonances. For the $\pi^- p \to \pi^0\pi^0$ the relevant isospin amplitudes are

$$\begin{aligned} \left\langle \Delta^0\pi^0|\pi^- p\right\rangle &= -\frac{1}{3}\sqrt{\frac{1}{5}}\ T^{\frac{3}{2}}_{\pi\Delta} + \frac{\sqrt{2}}{3}\ T^{\frac{1}{2}}_{\pi\Delta}, \\ \left\langle \sigma n|\pi^- p\right\rangle &= -\sqrt{\frac{2}{3}}\,T^{\frac{1}{2}}_{\sigma N}. \end{aligned} \tag{D1}$$

One can also perform an isospin decomposition of the $\pi N \to \pi\pi N$ reaction beyond isobar approximation. Within the $[1 \otimes 1] \otimes \frac{1}{2}$ scheme the isospin decomposition has the form:

$$\begin{aligned}
< \pi^0\pi^0 n|T|\pi^- p > &= \frac{2}{3}\sqrt{\frac{1}{5}}\,T_2^{\frac{3}{2}} + \frac{\sqrt{2}}{3}\,T_0^{\frac{1}{2}},\\
< \pi^+\pi^- n|T|\pi^- p > &= \frac{1}{3}\sqrt{\frac{1}{5}}\,T_2^{\frac{3}{2}} + \frac{1}{3}\,T_1^{\frac{3}{2}} - \frac{1}{3}\,T_1^{\frac{1}{2}} - \frac{\sqrt{2}}{3}\,T_0^{\frac{1}{2}},\\
< \pi^0\pi^- p|T|\pi^- p > &= -\sqrt{\frac{1}{10}}\,T_2^{\frac{3}{2}} - \frac{1}{3}\sqrt{\frac{1}{2}}\,T_1^{\frac{3}{2}} + \frac{\sqrt{2}}{3}\sqrt{\frac{1}{2}}\,T_1^{\frac{1}{2}},\\
< \pi^+\pi^+ n|T|\pi^+ p > &= \sqrt{\frac{4}{5}}\,T_2^{\frac{3}{2}},\\
< \pi^+\pi^0 p|T|\pi^+ p > &= -\sqrt{\frac{1}{10}}\,T_2^{\frac{3}{2}} - \sqrt{\frac{1}{2}}\,T_1^{\frac{3}{2}},
\end{aligned} \tag{D2}$$

where the upper subscript denotes the total isospin and the lower one stands for the isospin of the $\pi\pi$ subsystem. Thus the ρN-subchannel would only contribute to the $T_1^{\frac{3}{2}}$ and $T_1^{\frac{1}{2}}$ amplitudes. The independent isospin amplitudes $T_2^{\frac{3}{2}}$, $T_1^{\frac{3}{2}}$, $T_1^{\frac{1}{2}}$, $T_0^{\frac{1}{2}}$ correspond to the four irreducible representations of the isospin group and completely define isospin structure of the $\pi N \to 2\pi N$ transitions. The isospin amplitudes of Eq. (D2) can be expressed through the isobar ones Eq. (D1) as follows:

$$\begin{aligned}
T_2^{\frac{3}{2}} &= -\frac{1}{\sqrt{6}}\,T_{\pi\Delta}^{\frac{3}{2}},\\
T_0^{\frac{1}{2}} &= \sqrt{\frac{2}{3}}\,T_{\pi\Delta}^{\frac{1}{2}} - 2\sqrt{3}\,T_{\sigma N}^{\frac{1}{2}}.
\end{aligned} \tag{D3}$$

Appendix E: Interaction Lagrangians

In this Appendix we summarize the Lagrangian densities and decay widths of the baryonic resonances.

The πNN Lagrangian reads

$$\mathcal{L}_{\pi NN} = \frac{f_{\pi NN}}{m_\pi}\bar{u}_N[\gamma_\mu\gamma_5\boldsymbol{\tau}]u_N\partial^\mu\boldsymbol{\pi}. \tag{E1}$$

The πNN^* and σNN^* couplings of the $J^P = \frac{1}{2}^+$ resonance are

$$\mathcal{L}_{\varphi NN^*} = \frac{\mathrm{g}_{\varphi NN^*}}{m_\varphi}\bar{u}_{N^*}\begin{pmatrix}\gamma_5\\ \mathrm{i}\end{pmatrix}\gamma^\mu\tau_\varphi u_N\partial_\mu\varphi + h.c.; \tag{E2}$$

for the the $J^P = \frac{1}{2}^-$ resonance they are chosen in the form:

$$\mathcal{L}_{\varphi NN^*} = \frac{\mathrm{g}_{\varphi NN^*}}{m_\varphi} \bar{u}_{N^*} \begin{pmatrix} 1 \\ \mathrm{i}\gamma_5 \end{pmatrix} \tau_\varphi u_N \varphi + h.c., \tag{E3}$$

where $\varphi = \pi$, σ, $\tau_\pi = \boldsymbol{\tau}$, $\tau_\sigma = 1$, and the upper(lower) factor in the brackets correspond to the π-(σ-) meson.

The $\pi\pi\sigma$-coupling is described by

$$\mathcal{L}_{\pi\pi\sigma} = \mathrm{g}_{\pi\pi\sigma} m_\sigma \sigma(\boldsymbol{\pi}\boldsymbol{\pi}). \tag{E4}$$

The $\pi N\Delta$ coupling is defined as

$$\mathcal{L}_{\pi N^*\Delta} = \frac{\mathrm{g}_{\pi N\Delta}}{m_\pi} \bar{u}^\mu_\Delta \boldsymbol{T}\, u_N\, \partial_\mu \boldsymbol{\pi} + h.c., \tag{E5}$$

and Lagrangian density for the $N^* \to \pi\Delta(1232)$ transitions is given by

$$\mathcal{L}_{\pi N^*\Delta} = \frac{\mathrm{g}_{\pi N^*\Delta}}{m_\pi} \bar{u}^\mu_\Delta \boldsymbol{T} \begin{pmatrix} 1 \\ \mathrm{i}\gamma_5 \end{pmatrix} u_{N^*}\, \partial_\mu \boldsymbol{\pi} + h.c., \tag{E6}$$

where the upper(lower) factor in the brackets stands for the positive(negative)-parity nucleon resonance. The isospin transition factor $\boldsymbol{T}$ can be defined via the Clebsch-Gordan coefficient $\boldsymbol{T} = C^{\frac{3}{2} I_\Delta}_{\frac{1}{2}, I_N;\, 1\, I_\pi}$, where I_N, I_π, and I_Δ are isospin projections of the nucleon resonance, the pion, and $\Delta(1232)$ respectively. The decay width of the σ-meson, $\Gamma_\sigma(\mu^2_\sigma)$, and $\Delta(1232)$-isobar, $\Gamma_\Delta(\mu^2_\Delta)$, are readily obtained using Lagrangian desities Eqs. (E4, E6) as functions of the isobar masses. The isobar self-energy is a solution of the DSE-type equaiton Eq.(6). In the K-matirx approximation the imaginary part of the isobar self-energy can be expressed in terms of the isobar decay width as follows:

$$\begin{aligned} \mathrm{Im}\Sigma_\sigma(\mu^2_\sigma) &= \sqrt{\mu^2_\sigma}\, \Gamma_\sigma(\mu^2_\sigma), \\ \mathrm{Im}\Sigma_\Delta(\mu^2_\Delta) &= \sqrt{\mu^2_\Delta}\, \Gamma_\Delta(\mu^2_\Delta) \end{aligned} \tag{7}$$

The partial decay width of the $N^*(1525)$ and $N^*(1440)$ states are defined through as follows

$$\begin{aligned} \Gamma_{\sigma N} &= \int_{4m^2_\pi}^{(m_{N^*}-m_N)^2} \mathrm{d}\mu^2_\sigma A_\sigma(\mu^2_\sigma) \Gamma_{\sigma N}(\mu^2_\sigma), \\ \Gamma_{\pi\Delta} &= \int_{(m_N+m_\pi)^2}^{(m_{N^*}-m_\pi)^2} \mathrm{d}\mu^2_\Delta A_\sigma(\mu^2_\Delta) \Gamma_{\Delta N}(\mu^2_\Delta), \end{aligned} \tag{8}$$

coupling constant	N(1535)	N(1440)
$g_{\pi NN^*}$	0.5627	7.407
$g_{\sigma NN^*}$	0.00	-7.61
$g_{\pi N^*\Delta(1232)}$	0.00	7.68

TABLE III: Resonance coupling constants used in the calculatuions.

where the quantitites $\Gamma_{\sigma N}(\mu_\sigma^2)$ and $\Gamma_{\Delta N}(\mu_\Delta^2)$ can be readily evaluated from the couplings Eqs. (E2,E3, E6). The coupling constants used in the calculations are given in Table III.

[1] T. Feuster and U. Mosel, Phys. Rev. **C58**, 457 (1998).

[2] T. Feuster and U. Mosel, Phys. Rev. **C59**, 460 (1999).

[3] G. Penner and U. Mosel, Phys. Rev. **C66**, 055211 (2002).

[4] G. Penner and U. Mosel, Phys. Rev. **C66**, 055212 (2002).

[5] V. Shklyar, G. Penner, and U. Mosel, Eur. Phys. J. **A21**, 445 (2004).

[6] V. Shklyar, H. Lenske, and U. Mosel, Phys.Lett. **B650**, 172 (2007).

[7] V. Shklyar, H. Lenske, and U. Mosel, Phys.Rev. **C87**, 015201 (2013).

[8] X. Cao, V. Shklyar, and H. Lenske, Phys.Rev. **C88**, 055204 (2013).

[9] V. Shklyar, H. Lenske, and U. Mosel, Phys.Rev. **C72**, 015210 (2005).

[10] D. M. Manley, R. A. Arndt, Y. Goradia, and V. L. Teplitz, Phys. Rev. **D30**, 904 (1984).

[11] R. G. Edwards, J. J. Dudek, D. G. Richards, and S. J. Wallace, Phys.Rev. **D84**, 074508 (2011).

[12] S. Drr et al., Science **322**, 1224 (2008).

[13] H. Sanchis-Alepuz, G. Eichmann, S. Villalba-Chavez, and R. Alkofer, Phys.Rev. **D84**, 096003 (2011).

[14] R. Koniuk and N. Isgur, Phys. Rev. D **21**, 1868 (1980).

[15] S. Capstick and W. Roberts, Phys.Rev. **D58**, 074011 (1998).

[16] R. Arndt, W. Briscoe, I. Strakovsky, and R. Workman, Phys.Rev. **C74**, 045205 (2006).

[17] R. Cutkosky, C. Forsyth, R. Hendrick, and R. Kelly, Phys.Rev. **D20**, 2839 (1979).

[18] G. Hoehler, PiN Newslett. **9**, 1 (1993).

[19] A. Anisovich et al., Eur.Phys.J. **A48**, 15 (2012).

[20] Particle Data Group, J. Beringer et al., Phys.Rev. **D86**, 010001 (2012).

[21] R. A. Arndt, J. M. Ford, and L. D. Roper, Phys.Rev. **D32**, 1085 (1985).

[22] R. Cutkosky and S. Wang, Phys.Rev. **D42**, 235 (1990).

[23] M. Doring, C. Hanhart, F. Huang, S. Krewald, and U.-G. Meissner, Nucl.Phys. **A829**, 170 (2009).

[24] N. Suzuki et al., Phys.Rev.Lett. **104**, 042302 (2010).

[25] Crystal Ball Collaboration, K. Craig et al., Phys.Rev.Lett. **91**, 102301 (2003).

[26] Crystal Ball Collaboration, S. Prakhov et al., Phys.Rev. **C69**, 045202 (2004).

[27] T. Skorodko et al., Eur.Phys.J. **A35**, 317 (2008).

[28] M. Shrestha and D. Manley, Phys.Rev. **C86**, 055203 (2012).

[29] Crystal Ball Collaboration, S. Prakhov et al., Phys. Rev. C **72**, 015203 (2005).

[30] D. Manley and E. Saleski, Phys.Rev. **D45**, 4002 (1992).

[31] T. Vrana, S. Dytman, and T. Lee, Phys.Rept. **328**, 181 (2000).

[32] R. Cutkosky et al., Phys.Rev. **D20**, 2804 (1979).

[33] A. Sarantsev et al., Phys.Lett. **B659**, 94 (2008).

[34] H. Haberzettl, K. Nakayama, and Y. Oh, Few Body Syst. **54**, 1141 (2013).

[35] O. Krehl, C. Hanhart, S. Krewald, and J. Speth, Phys.Rev. **C62**, 025207 (2000).

[36] D. Ronchen et al., Eur.Phys.J. **A49**, 44 (2013).

[37] H. Kamano and M. Arima, Phys.Rev. **C73**, 055203 (2006).

[38] N. Fettes, V. Bernard, and U. G. Meissner, Nucl.Phys. **A669**, 269 (2000).

[39] V. Bernard, N. Kaiser, and U. G. Meissner, Nucl.Phys. **B457**, 147 (1995).

[40] V. Bernard, N. Kaiser, and U.-G. Meissner, Nucl.Phys. **A619**, 261 (1997).

[41] N. Mobed, J. Zhang, and D. Singh, Phys.Rev. **C72**, 045204 (2005).

[42] D. Siemens, V. Bernard, E. Epelbaum, H. Krebs, and U.-G. Meiner, Phys.Rev. **C89**, 065211 (2014).

[43] S. Schneider, S. Krewald, and U.-G. Meissner, Eur.Phys.J. **A28**, 107 (2006).

[44] E. Oset and M. Vicente-Vacas, Nucl.Phys. **A446**, 584 (1985).

[45] A. Matsuyama, T. Sato, and T.-S. Lee, Phys.Rept. **439**, 193 (2007).

[46] H. Kamano, B. Julia-Diaz, T.-S. Lee, A. Matsuyama, and T. Sato, Phys.Rev. **C79**, 025206 (2009).

[47] H. Kamano, Phys.Rev. **C88**, 045203 (2013).

[48] H. Kamano, S. Nakamura, T. S. H. Lee, and T. Sato, Phys.Rev. **C88**, 035209 (2013).

[49] B. C. Pearce and B. K. Jennings, Nucl. Phys. **A528**, 655 (1991).

[50] C. Deutsch-Sauermann, B. Friman, and W. Norenberg, Phys. Lett. **B409**, 51 (1997).

[51] E. Hernández, E. Oset, and M. J. Vicente Vacas, Phys. Rev. C **66**, 065201 (2002).

[52] L.-B. I/12a, Springer-Verlag **ISBN: 978-3-540-18386-0**, 1 (1988).

[53] CLAS Collaboration, V. Mokeev et al., Phys.Rev. **C86**, 035203 (2012).

[54] V. Shklyar, H. Lenske, U. Mosel, and G. Penner, Phys. Rev. **C71**, 055206 (2005).

[55] HADES, http://www-hades.gsi.de/.

[56] JPARC, http://j-parc.jp/Hadron/en/index.html.

[57] M. Jacob and G. C. Wick, Ann. Phys. **7**, 404 (1959).